Eur. Phys. J. C 21, 683–700 (2001)
Digital Object Identifier (DOI) 10.1007/s100520100767

THE EUROPEAN PHYSICAL JOURNAL C

Extended minimal flavour violating MSSM and implications for B physics

A. Ali[a], E. Lunghi[b]

Deutsches Elektronen Synchrotron, DESY, Notkestrasse 85, 22607 Hamburg, Germany

Received: 20 May 2001 / Revised version: 5 August 2001 /
Published online: 31 August 2001 –

Abstract. The recently reported measurements of the CP asymmetry $a_{\psi K}$ by the BABAR and BELLE collaborations, obtained from the rate differences in the decays $B^0 \to (J/\psi K_s), (J/\psi K_L)$ etc., and their charge conjugates, are in good agreement with the standard model (SM) prediction of the same, resulting from the unitarity of the CKM matrix. The so-called minimal flavour violating (MFV) supersymmetric extensions of the standard model, in which the CKM matrix remains the only flavour changing structure, predict $a_{\psi K}$ similar to the one in the SM. With the anticipated precision in $a_{\psi K}$ and other CP asymmetries at the B factories and hadron colliders, one hopes to pin down any possible deviation from the SM. We discuss an extension of the MFV-supersymmetric models which comfortably accommodates the current measurements of the CP asymmetry $a_{\psi K}$, but differs from the SM and the MFV-supersymmetric models due to an additional flavour changing structure beyond the CKM matrix. We suggest specific tests in forthcoming experiments in B physics. In addition to the CP-asymmetries in B-meson decays, such as $a_{\psi K}$ and $a_{\pi\pi}$, and the mass difference ΔM_s in the B_s^0 - $\overline{B_s^0}$ system, we emphasize measurements of the radiative transition $b \to d\gamma$ as sensitive probes of the postulated flavour changing structure. This is quantified in terms of the ratio $R(\rho\gamma/K^*\gamma) = 2\mathcal{B}(B^0 \to \rho^0\gamma)/\mathcal{B}(B^0 \to K^{*0}\gamma)$, the isospin violating ratio $\Delta^{\pm 0} = \mathcal{B}(B^\pm \to \rho^\pm\gamma)/2\mathcal{B}(B^0 \to \rho^0\gamma) - 1$, and the CP-asymmetry in the decay rates for $B^+ \to \rho^+\gamma$ and its charge conjugate. Interestingly, the CKM–unitarity analysis in the Extended–MFV model also allows solutions $\bar\rho < 0$ for the Wolfenstein parameter, as opposed to the SM and the MFV-supersymmetric models for which only $\bar\rho > 0$ solutions are now admissible, implying $\gamma > \pi/2$, where $\gamma = -\arg V_{ub}$. Such large values of γ are hinted by the current measurements of the branching ratios for the decays $B \to \pi\pi$ and $B \to K\pi$.

1 Introduction

With the advent of the B-factory era, the principal focus in flavour physics is now on measuring CP-violating asymmetries, which will determine the inner angles α, β, and γ of the unitarity triangle (UT) in the Cabibbo-Kobayashi-Maskawa (CKM) theory [1]. A beginning along this road has already been made through the impressive measurements of $\sin 2\beta$ by the B-factory experiments BABAR [2] and BELLE [3], following earlier leads from the OPAL [4], CDF [5,6], and ALEPH [7] collaborations. The principal decay modes used in the measurement of $\sin 2\beta$ are $B_d^0 \to J/\psi K_S$, $B_d^0 \to \psi(2S)K_S$, $B_d^0 \to J/\psi K_L$, and their charge conjugates. Concentrating on the decays $B_d^0/\overline{B_d^0} \to J/\psi K_s$, the time-dependent CP-asymmetry $a_{\psi K_S}(t)$ can be expressed as follows:

$$a_{\psi K_S}(t) \equiv \frac{\Gamma(B_d^0(t) \to J/\psi K_S) - \Gamma(\overline{B_d^0}(t) \to J/\psi K_S)}{\Gamma(B_d^0(t) \to J/\psi K_S) + \Gamma(\overline{B_d^0}(t) \to J/\psi K_S)}$$
$$= \mathcal{A}_{\rm CP}^{\rm dir}\cos(\Delta M_{B_d}t) + \mathcal{A}_{\rm CP}^{\rm mix}\sin(\Delta M_{B_d}t)\,, \quad (1)$$

where the states $B_d^0(t)$ and $\overline{B_d^0}(t)$ are understood as evolving from the corresponding initial flavour eigenstates (i.e., at $t = 0$), and ΔM_{B_d} is the mass difference between the two mass eigenstates of the B_d^0 -$\overline{B_d^0}$ system, known very precisely, thanks in part due to the BABAR [8] and BELLE [9] measurements, and the present world average is $\Delta M_{B_d} = 0.484 \pm 0.010$ (ps)$^{-1}$ [10]. The quantities $\mathcal{A}_{\rm CP}^{\rm dir}$ and $\mathcal{A}_{\rm CP}^{\rm mix}$ are called the direct (i.e., emanating from the decays) and mixing-induced CP-asymmetries, respectively. Of these, the former is CKM-suppressed - a result which holds in the SM. The expectation $\mathcal{A}_{\rm CP}^{\rm dir}/\mathcal{A}_{\rm CP}^{\rm mix} \ll 1$ is supported by present data on direct CP-asymmetry in charged B-decays, $B^\pm \to J/\psi K^\pm$, yielding an upper bound on $\mathcal{A}_{\rm CP}^{\rm dir}$ which is already quite stringent [2,3]. Hence, we shall assume that direct CP-asymmetry in $a_{\psi K_S}(t)$ is negligible and neglect the first term on the r.h.s. of (1). Recalling that $\mathcal{A}_{\rm CP}^{\rm mix}$ is a pure phase, one has in the SM $\mathcal{A}_{\rm CP}^{\rm mix} = \eta_{J/\psi K_S} a_{\psi K_S}$, with $\eta_{(J/\psi K_S)} = -1$ being the intrinsic CP-parity of the $J/\psi K_S$ state, (1) simplifies to

$$a_{\psi K_S}(t) = -a_{\psi K_S}\sin(\Delta M_{B_d}t)\,. \quad (2)$$

[a] e-mail: ali@x4u2.desy.de
[b] e-mail: lunghi@mail.desy.de

This relation is essentially free of hadronic uncertainties. Hence, a measurement of the left-hand-side allows to extract $a_{\psi K_S}$ cleanly. Note that in the SM $a_{\psi K_S} = \sin 2\beta$. The present world average of this quantity is [2–7]

$$a_{\psi K_S} = 0.79 \pm 0.12 \ , \tag{3}$$

which is dominated by the BABAR ($a_{\psi K_S} = 0.59 \pm 0.14$ (stat) ± 0.05(syst)) [2] and BELLE ($a_{\psi K_S} = 0.99 \pm 0.14$ (stat) ± 0.06(syst)) [3] results. We note that the current world average (which includes a scale factor following the Particle Data Group prescription [11]) based on all five experiments yields a value of $a_{\psi K_S}$ which is different from a null result by more than six standard deviations. To test the consistency of the SM, the current experimental value of $a_{\psi K_S}$ in (3) is to be compared with the indirect theoretical estimates of the same obtained from the unitarity of the CKM matrix. These latter values lie typically in the range $a^{\rm SM}_{\psi K_S} = 0.6 - 0.8$ (at 68% C.L.) [12–19], where the spread reflects both the uncertainties in the input parameters and treatment of errors, with most analyses yielding $a^{\rm SM}_{\psi K_S} \simeq 0.70$ as the central value of the CKM fits. We conclude that he current measurements of $a_{\psi K_S}$ are in good agreement with its indirect estimates in the SM.

The consistency of the SM with experiments on CP-violation in B-decays will come under minute scrutiny, with greatly improved accuracy on $a_{\psi K_S}$ and measurements of the other two angles of the UT, α and γ at the e^+e^- and hadronic B-factories. In addition, a large number of direct CP-asymmetries in charged and neutral B-decays, as well as flavour-changing-neutral-current (FCNC) transitions in B- and K-decays, which will be measured in the course of the next several years, will greatly help in pinning down the underlying theory of flavour physics. It is conceivable that precision experiments in flavour physics may force us to revise the SM framework by admitting new interactions, including the possibility of having new CP-violating phases. Some alternatives yielding a lower value of $a_{\psi K_S}$ than in the SM have already been entertained in the literature [20–22]. With the experimental situation now crystallized in (3), it now appears that the CP-asymmetry $a_{\psi K_S}$ has a dominantly SM origin.

In popular extensions of the SM, such as the minimal supersymmetric standard model (MSSM), one anticipates supersymmetric contributions to FCNC processes, in particular ΔM_{B_d}, ΔM_{B_s} (the mass difference in the B^0_s -$\overline{B^0_s}$ system), and ϵ_K, characterizing $\mathcal{A}^{\rm mix}_{\rm CP}$ in the K^0 -$\overline{K^0}$ system. However, if the CKM matrix remains effectively the only flavour changing (FC) structure, which is the case if the quark and squark mass matrices can be simultaneously diagonalized (equivalently, the off-diagonal squark mass matrix elements are small at low energy scale), and all other FC interactions are associated with rather high scales, then all hadronic flavour transitions can be interpreted in terms of the same unitarity triangles which one encounters in the SM. In particular, in these theories $a_{\psi K_s}$ measures the same quantity $\sin 2\beta$ as in the SM. These models are usually called the minimal flavour violating (MFV) models, following [23]. Despite the intrinsic dependence of the mass differences ΔM_{B_d}, ΔM_{B_s}, and ϵ_K on the underlying supersymmetric parameters, the MFV models remain very predictive and hence they have received a lot of theoretical attention lately [15,23–29]. To summarize, in these models the SUSY contributions to ΔM_{B_d}, ΔM_{B_s}, and ϵ_K have the same CKM-dependence as the SM top quark contributions in the box diagrams (denoted below by C_1^{Wtt}). Moreover, supersymmetric effects are highly correlated and their contributions in the quantities relevant for the UT-analysis can be effectively incorporated in terms of a single common parameter f by the following replacement [24,25]:

$$\epsilon_K,\ \Delta M_{B_s}\ \Delta M_{B_d},\ a_{\psi K_S} : C_1^{Wtt} \to C_1^{Wtt}(1+f) \ . \tag{4}$$

The parameter f is positive definite and real, implying that there are no new phases in any of the quantities specified above. The size of f depends on the parameters of the supersymmetric models and the model itself [30–33]. Given a value of f, the CKM unitarity fits can be performed in these models much the same way as they are done for the SM. Qualitatively, the CKM-fits in MFV models yield the following pattern for the three inner angles of the UT:

$$\beta^{\rm MFV} \simeq \beta^{\rm SM} \ ; \ \ \gamma^{\rm MFV} < \gamma^{\rm SM} \ ; \ \ \alpha^{\rm MFV} > \alpha^{\rm SM} \ . \tag{5}$$

For example, a recent CKM-fit along these lines yields the following central values for the three angles [15]:

$$\begin{aligned} &f = 0 \ (\text{SM}): \ (\alpha,\beta,\gamma)_{\rm central} = (95^\circ, 22^\circ, 63^\circ) \ , \\ &f = 0.4 \ (\text{MFV}): \ (\alpha,\beta,\gamma)_{\rm central} = (112^\circ, 20^\circ, 48^\circ) \ , \end{aligned} \tag{6}$$

leading to $(\sin 2\beta)^{\rm SM}_{\rm central} \simeq 0.70$ and $(\sin 2\beta)^{\rm MFV}_{\rm central} \simeq 0.64$. Thus, what concerns $\sin 2\beta$, the SM and the MFV models give similar results from the UT-fits, unless much larger values for the parameter f are admitted which, as argued in [30–33] and in this paper, is unlikely due to the existing constraints on the MFV-SUSY parameters.

However, in a general extension of the SM, one expects that all the quantities appearing on the l.h.s. in (4) will receive independent additional contributions. In this case, the magnitude and the phase of the off-diagonal elements in the B^0_d -$\overline{B^0_d}$ and B^0_s - $\overline{B^0_s}$ mass matrices can be parametrized as follows [34,35]:

$$\begin{aligned} M_{12}(B_d) &= \frac{\langle \bar{B}_d | H_{eff}^{\Delta B=2} | B_d \rangle}{2M_{B_d}} = r_d^2 e^{2i\theta_d} M_{12}^{SM}(B_d) \ , \\ M_{12}(B_s) &= \frac{\langle \bar{B}_s | H_{eff}^{\Delta B=2} | B_s \rangle}{2M_{B_s}} = r_s^2 e^{2i\theta_s} M_{12}^{SM}(B_s) \ , \end{aligned} \tag{7}$$

where r_d (r_s) and θ_d (θ_d) characterize, respectively, the magnitude and the phase of the new physics contribution to the mass difference ΔM_{B_d} (ΔM_{B_s}). It follows that a measurement of $a_{\psi K_s}$ would not measure $\sin 2\beta$, but rather a combination $\sin 2(\beta + \theta_d)$. Likewise, a measurement of the CP asymmetry in the decays $B^0_d \to \pi\pi$ and its charge conjugate, $a_{\pi\pi}$, (assuming that the penguin contributions are known) would not measure $\sin 2\alpha$, but rather $\sin 2(\alpha - \theta_d)$. Very much along the same lines, the decay

$B_s \to J/\psi\phi$ and its charge conjugate would yield a CP asymmetry $a_{\psi\phi} \simeq -\sin(\delta - \theta_s)$, where $\delta \simeq 1/2\lambda^2 \simeq 0.02$ in the SM, and $\lambda \simeq 0.22$ is one of the four CKM parameters in the Wolfenstein representation [36]. Thus, the phase θ_s could enhance the CP-asymmetry $a_{\psi\phi}$ bringing it within reach of the LHC-experiments [37]. In this scenario, one also expects new contributions in $M_{12}(K^0)$, bringing in their wake additional parameters $(r_\epsilon,\ \theta_\epsilon)$. They will alter the profile of CP-violation in the decays of the neutral kaons. In fact, sizable contributions from the supersymmetric sector have been entertained in the literature, though it appears now unlikely that ϵ_K and/or ϵ'_K/ϵ_K (which is a measure of direct CP violation in the neutral Kaon decays) are saturated by supersymmetry [38,39].

It is obvious that in such a general theoretical scenario, which introduces six *a priori* independent parameters, the predictive power vested in the CKM-UT analysis is lost. We would like to retain this predictivity, at least partially, and entertain a theoretical scenario which accommodates the current measurement in flavour physics, including the recent measurements of $a_{\psi K_S}$, but admits additional flavour structure. A model which incorporates these features is introduced and discussed in Sect. 2, using the language of minimal insertion approximation (MIA) [40] in a supersymmetric context. In this framework, gluinos are assumed heavy and hence have no measurable consequences for low energy phenomenology. All FC transitions which are not generated by the CKM mixing matrix are proportional to the properly normalized off–diagonal elements of the squark mass matrices:

$$(\delta_{ij})^{U,D}_{AB} \equiv \frac{(M^2_{ij})^{U,D}_{AB}}{M_{\tilde{q}_i} M_{\tilde{q}_j}} \tag{8}$$

where $i,j = 1,2,3$ and $A,B = L,R$. We give arguments why we expect that the dominant effect of the non-CKM structure contained in the MIA-parameters is expected to influence mainly the $b \to d$ and $s \to d$ transitions while the $b \to s$ transition is governed by the MFV-SUSY and the SM contributions alone. For what concerns the quantities entering in the UT analysis, the following pattern for the supersymmetric contributions emerges in this model:

$$\Delta M_{B_s} : C_1^{Wtt} \to C_1^{Wtt}(1+f) \tag{9}$$

$$\epsilon_K,\ \Delta M_{B_d},\ a_{\psi K_S} : C_1^{Wtt} \to C_1^{Wtt}(1+f) + C_1^{MI} \equiv C_1^{Wtt}\,(1+f+g) \tag{10}$$

where the parameters f and $g = g_R + i g_I$ represent normalized (w.r.t. the SM top quark Wtt) contributions from the MFV and MIA sectors, respectively. Thus, in the UT-analysis the contribution from the supersymmetric sector can be parametrized by two real parameters f and g_R and a parameter g_I, generating a phase θ_d, which is in general non-zero due to the complex nature of the appropriate mass insertion parameter. We constrain these parameters, taking into account all direct and indirect bounds on the supersymmetric parameters, including the measured rates for $b \to s\gamma$ decay [41–43], $(g-2)_\mu$ from the Brookhaven experiment [44], and the present bound on the $b \to d\gamma$ transition, following from the experimental bound on the ratio of the branching ratios $R(\rho\gamma/K^*\gamma) = 2\mathcal{B}(B^0 \to \rho^0\gamma)/\mathcal{B}(B^0 \to K^{*0}\gamma)$ [45]. We do not include the quantity ϵ'_K/ϵ_K in our analysis, despite its impeccable measurement by the NA48 [46] and KTeV [47] Collaborations, yielding the present world average $\mathrm{Re}\,\epsilon'_K/\epsilon_K = (1.7 \pm 0.2) \times 10^{-3}$, due to the inherent non–perturbative uncertainties which have greatly reduced the impact of the ϵ'_K/ϵ_K measurement on the CKM phenomenology (see, for a recent review, [17]).

This model, called henceforth the Extended-MFV model, leads to a number of testable consequences, some of which are common with the more general scenarios discussed earlier in the context of (7) [34,35]. Thus, for a certain range of the argument of the MIA parameter, this model yields $a_{\psi K_s} < a_{\psi K_s}^{\mathrm{SM/MFV}}$. For other choices of the model parameters, this model yields a higher value for this CP asymmetry. A precise measurement of $a_{\psi K_s}$ would fix this argument $(= \theta_d)$ and we show its allowed range suggested by the current data. Likewise, the CP-asymmetry $a_{\pi\pi} = \sin 2(\alpha - \theta_d)$ will be shifted from its SM-value, determined by θ_d. All $b \to d$ transitions (leading to the decays such as $b \to d\gamma$, $b \to d\ell^+\ell^-$, $B^0_d \to \ell^+\ell^-$, where $\ell^\pm = e^\pm, \mu^\pm, \tau^\pm$, and the ratio of the mass differences $\Delta M_{B_s}/\Delta M_{B_d}$) may turn out to be significantly different from their SM and MFV counterparts. To illustrate this, we work out in detail the implications for the exclusive decays $B \to \rho^0\gamma$ and $B^\pm \to \rho^\pm\gamma$, concentrating on the (theoretically more reliable) ratios $R(\rho\gamma/K^*\gamma) \equiv 2\mathcal{B}(B^0 \to \rho^0\gamma)/\mathcal{B}(B^0 \to K^*\gamma)$, the isospin violating ratio $\Delta^{\pm 0} \equiv \mathcal{B}(B^\pm \to \rho^\pm\gamma)/2\mathcal{B}(B^0 \to \rho^0\gamma) - 1$, and direct CP-asymmetry in the decay rates for $B^- \to \rho^-\gamma$ and its charge conjugate. We also find that the fits of the CKM unitarity triangle in the extended MFV model, characterized by (9) and (10) above, admit both $\bar\rho > 0$ and $\bar\rho < 0$ solutions, where $\bar\rho$ is one of the Wolfenstein parameters [36]. We illustrate this by working out the predicted values of γ (and α) and ΔM_{B_s} in this model for some specific choice of the parameters. This is in contrast with the corresponding fits in the SM and the MFV–MSSM models, which currently yield $\bar\rho > 0$ at 2 standard deviations in the SM, with the significance increasing in the MFV–MSSM models. The allowed CKM–fits in the extended–MFV model with $\bar\rho < 0$ imply in turn $\gamma > \pi/2$. We note that such large values of γ are hinted by phenomenological analyses [48, 49] of the current measurements of the branching ratios for the decays $B \to K\pi,\ \pi\pi$ [50–52]. However, this inference is not yet convincing due to the present precision of data and lack of a reliable estimate of non–perturbative final state interactions in these decays.

This paper is organized as follows: In Sect. 2, we give the outline of our extended-MFV model.The supersymmetric contributions to the quantities of interest (ϵ_K, ΔM_{B_s}, ΔM_{B_d}, $a_{\psi K_S}$) and $R(\rho\gamma/K^*\gamma)$ are discussed in Sect. 3, where we also discuss the impact of the $(g-2)_\mu$ experiment on our analysis. Numerical analysis of the parameters $(f, |g|)$, taking into account the experimental constraints from the $b \to s\gamma$, $b \to d\gamma$ and $(g-2)_\mu$, is presented in Sect. 4. A comparative analysis of the uni-

tarity triangle in the SM, MFV and the Extended-MFV models is described in Sect. 5, where we also show the resulting constraints on the parameters g_R and g_I and the CP-asymmetry $a_{\psi K_s}$. The impact of the Extended-MFV model on the $b \to d\gamma$ transitions are worked out in Sect. 6. Section 7 contains a summary and some concluding remarks. The explicit stop and chargino mass matrices are displayed in Appendix A and some loop functions encountered in the supersymmetric contributions are given in Appendix B.

2 Outline of the model

The supersymmetric model that we consider is a generalization of the model proposed in [23], based on the assumptions of Minimal Flavour Violation with heavy squarks (of the first two generations) and gluinos. The charged Higgs and the lightest chargino and stop masses are required to be heavier than 100 GeV in order to satisfy the lower bounds from direct searches. The rest of the SUSY spectrum is assumed to be almost degenerate and heavier than 1 TeV. In this framework the lightest stop is almost right–handed and the stop mixing angle (which parameterizes the amount of the left-handed stop $\tilde{t}_L$ present in the lighter mass eigenstate) turns out to be of order $O(M_W/M_{\tilde{q}}) \simeq 10\%$; for definiteness we will take $|\theta_{\tilde{t}}| \leq \pi/10$.

The assumption of a heavy (≥ 1 TeV) gluino totally suppresses any possible gluino–mediated SUSY contribution to low energy observables. On the other hand, the presence of only a single light squark mass eigenstate (out of twelve) has strong consequences due to the rich flavour structure which emerges from the squark mass matrices. As discussed in the preceding section, adopting the MIA-framework [40], all the FC effects which are not generated by the CKM mixing matrix are proportional to the properly normalized off–diagonal elements of the squark mass matrices (see (8)). In order to take into account the effect of a light stop, we exactly diagonalize the 2×2 stop system and adopt the slightly different MIA implementation proposed in [53]. In this approach, a diagram can contribute sizably only if the inserted mass insertions involve the light stop. All other diagrams require necessarily a loop with at least two heavy (≥ 1 TeV) squarks and are therefore automatically suppressed. This leaves us with only two unsuppressed flavour changing sources other than the CKM matrix, namely the mixings $\tilde{u}_L - \tilde{t}_2$ (denoted by $\delta_{\tilde{u}_L\tilde{t}_2}$) and $\tilde{c}_L - \tilde{t}_2$ (denoted by $\delta_{\tilde{c}_L\tilde{t}_2}$). We note that $\delta_{\tilde{u}_L\tilde{t}_2}$ and $\delta_{\tilde{c}_L\tilde{t}_2}$ are mass insertions extracted from the up–squarks mass matrix after the diagonalization of the stop system and are therefore linear combinations of $(\delta_{13})^U_{LR}$, $(\delta_{13})^U_{LL}$ and of $(\delta_{23})^U_{LR}$, $(\delta_{23})^U_{LL}$, respectively.

Finally, a comment on the normalization that we adopt for the mass insertions is in order. In [54] it has been pointed out that $(\delta_{i3})^U_{LR}$ must satisfy an upper bound of order $2m_t/M_{\tilde{q}_i}$ in order to avoid charge and colour breaking minima and directions unbounded from below in the scalar potential. We normalize the insertions relevant to our discussion so that, in the limit of light stop, they automatically satisfy this constraint:

$$\delta_{\tilde{u}(\tilde{c})_L\tilde{t}_2} \equiv \frac{M^2_{\tilde{u}(\tilde{c})_L\tilde{t}_2}}{M_{\tilde{t}_2}M_{\tilde{q}}}\frac{|V_{td(s)}|}{V^*_{td(s)}}\,. \tag{11}$$

This definition includes the phase of the CKM element $V_{td(s)}$. In this way, deviations from the SM predictions, for what concerns CP violating observables, will be mainly associated with complex values of the mass insertion parameters. For instance, as we will argue in the following, the CP asymmetry $a_{\psi K_S}$ in the decay $B \to J/\psi K_s$ can differ from the SM expectation only if $\arg\delta_{\tilde{u}_L\tilde{t}_2} \neq 0$. In general, the two phases must not be aligned with the respective SM-phases entering in the box diagram:

$$\arg\frac{M^2_{\tilde{u}(\tilde{c})_L\tilde{t}_2}}{M_{\tilde{t}_2}M_{\tilde{q}}} \neq \arg V^*_{td(s)}\,. \tag{12}$$

The insertion $\delta_{\tilde{c}_L\tilde{t}_2}$ characterizes the $b \to s$ transitions and it enters in the determination of the $B_s - \bar{B}_s$ mass difference, the $b \to s\gamma$ decay rate, and observables related to other FCNC decays such as $b \to s\ell^+\ell^-$. For what concerns the $b \to s\gamma$ decay, previous analyses [55] pointed out that contributions proportional to this insertion can be as large as the SM one. The experimental results for the inclusive branching fraction are

$$\mathcal{B}(B \to X_s\gamma) = \begin{cases} (3.19 \pm 0.43_{stat} \pm 0.27_{syst}) \times 10^{-4} \\ \quad \text{CLEO [41]} \\ (3.11 \pm 0.80_{stat} \pm 0.72_{syst}) \times 10^{-4} \\ \quad \text{ALEPH [42]} \\ (3.36 \pm 0.53_{stat} \pm 42_{syst} \pm (^{0.50}_{0.54})_{model}) \times 10^{-4} \\ \quad \text{BELLE [43].} \end{cases} \tag{13}$$

Combining these results and adding the errors in quadrature we obtain the following world average for the inclusive branching ratio

$$\mathcal{B}(B \to X_s\gamma) = (3.22 \pm 0.40) \times 10^{-4} \tag{14}$$

yielding the following 95% C.L. experimentally allowed range

$$2.41 \times 10^{-4} \leq \mathcal{B}(B \to X_s\gamma) \leq 4.02 \times 10^{-4}\,. \tag{15}$$

Using the LO theoretical expression for this branching ratio, the following bound is obtained:

$$0.30 \leq \left|C_7^{eff,LO}(m_b)\right| \leq 0.40 \tag{16}$$

where $C_7^{eff,LO}(m_b)$ is the relevant Wilson coefficient evaluated in the LL approximation and has the value -0.316 in the SM. Analyses of the NLO SM [56] and SUSY [57, 23, 58, 59] contributions (for the latter only a limited class of SUSY models were considered) showed that the LO result can receive substantial corrections. Notice that the

NLO analysis presented in [57,23,58,59] is valid exactly for the class of models that we consider over all the SUSY parameter space (including the large $\tan\beta$ region). Implementing their formulae and allowing the SUSY input parameters to vary within the range that we will further discuss in Sect. 4, we find that, up to few percents, the branching ratio is given by

$$\mathcal{B}(B\to X_s\gamma) = 22.23\ \left[C_7^{eff,NLO}(m_b) - 0.061\right]^2 + 0.264\ , \tag{17}$$

$$C_7^{eff,NLO}(m_b) = -0.175 + 0.666\ C_7^{eff,NLO}(M_W) + 0.093\ C_8^{eff,NLO}(M_W)\ . \tag{18}$$

The explicit expressions for $C_{7,8}^{eff,NLO}(M_W)$ can be found in [57,23,58,59]. Combining (17) and the bound (15), we obtain

$$-0.35 \le C_7^{eff,NLO}(m_b) \le -0.24 \quad \text{or} \quad 0.36 \le C_7^{eff,NLO}(m_b) \le 0.49\ . \tag{19}$$

Notice that in [58,59] it is pointed out that in order to get a result stable against variations of the heavy SUSY particles scale, it is necessary to properly take into account all possible SUSY contributions and to resum all the large logarithms that arise. The inclusion of the insertion $\delta_{\tilde{c}_L\tilde{t}_2}$ in this picture, in particular, should not be limited to the LO matching conditions but should instead extend to the complete NLO analysis. This program is clearly beyond the scope of the present paper. Moreover, one finds that, including the NLO corrections, the SM almost saturates the experimental branching ratio. In view of this we choose not to consider $\delta_{\tilde{c}_L\tilde{t}_2}$ in our analysis. Of course, the SUSY contribution from the MFV sector is still there, but it is real relative to the SM. The assumption of neglecting $\delta_{\tilde{c}_L\tilde{t}_2}$ will be tested in CP-asymmetries $\mathcal{A}_{\rm CP}(b\to s\gamma)$ and $\mathcal{A}_{\rm CP}(B\to K^*\gamma)$ at the B-factories. Notice that the exclusion of $\delta_{\tilde{c}_L\tilde{t}_2}$ from our analysis introduces strong correlations between the physics that governs $b\to d$ and $b\to s$ transitions, such as the ratio $\Delta M_{B_s}/\Delta M_{B_d}$, which would deviate from its SM (and MFV model) values.

The free parameters of the model are the common mass of the heavy squarks and gluino ($M_{\tilde{q}}$), the mass of the lightest stop ($M_{\tilde{t}_2}$), the stop mixing angle ($\theta_{\tilde{t}}$), the ratio of the two Higgs vevs ($\tan\beta_S$ [1]), the two parameters of the chargino mass matrix (μ and M_2), the charged Higgs mass ($M_{H^\pm}$) and $\delta_{\tilde{u}_L\tilde{t}_2}$. All these parameters are assumed to be real with the only exception of the mass insertion whose phase in not restricted *a priori*. In this way we avoid any possible problem with too large contributions to flavour conserving CP violating observables like the electric dipole moments of the leptons, hadrons and atoms.

In the next section we analyze the structure of the SUSY contributions to the observables related to the determination of the unitarity triangle, namely ϵ_K, $\Delta M_{d,s}$ and $a_{\psi K_S}$.

[1] We adopt the notation β_S in order not to generate confusion with the inner angle of the unitarity triangle which is denoted by β

3 SUSY contributions

The effective Hamiltonian that describes $\Delta F = 2$ transitions can be written as

$$\mathcal{H}_{eff}^{\Delta F=2} = -\frac{G_F^2 M_W^2}{(2\pi)^2}(V_{tq_1}V_{tq_2}^*)^2\,(C_1(\mu)\ \bar{q}_{2L}^\alpha\gamma^\mu q_{1L}^\alpha \cdot \bar{q}_{2L}^\beta\gamma_\mu q_{1L}^\beta\ +\ C_2(\mu)\ \bar{q}_{2L}^\alpha q_{1R}^\alpha\cdot\bar{q}_{2L}^\beta q_{1R}^\beta + C_3(\mu)\ \bar{q}_{2L}^\alpha q_{1R}^\beta\cdot\bar{q}_{2L}^\beta q_{1R}^\alpha\Big) + h.c.\ , \tag{20}$$

where α,β are colour indices and $(q_1,q_2) = (s,d)$, (b,d), (b,s) for the K, B_d and B_s systems respectively.

In this framework, as previously explained, gluino contributions are negligible; therefore, we have to deal only with charged Higgs (which obeys the SM CKM structure) and chargino mediated box diagrams. Let us comment on the latter. The dominant graphs must involve exclusively the lightest stop eigenstate since the presence of an heavy (≥ 1 TeV) sparticle would definitely suppress their contribution. Moreover, Feynman diagrams that contribute to C_3 are substantially suppressed with respect to diagrams that contributes to C_1. In fact, for what concerns the B system, the vertices $b_R-\tilde{H}-\tilde{t}_2$ and $b_L-\tilde{H}-\tilde{t}_2$ are proportional, respectively, to $m_b\sin\theta_{\tilde{t}}/(\sqrt{2}M_W\cos\beta_S)$ and $m_t\cos\theta_{\tilde{t}}/(\sqrt{2}M_W\sin\beta_S)$. Their ratio is thus of order $(m_b/m_t\tan\beta_S\tan\theta_{\tilde{t}})^2$ which, even in the large $\tan\beta_S$ regime, is damped and not much larger than $O(0.1)$. In the K system m_b must be replaced by m_s and the suppression is even stronger. Notice that in frameworks in which the split between the two stop mass eigenstates is not so marked, this argument fails. Diagrams mediated by the exchange of both stops must be considered and it is possible to find regions of the parameter space (for large $\tan\beta_S$) in which SUSY contributions to C_3 are indeed dominant [38]. We note that, the $\tan^4\beta_S$ enhanced neutral Higgs contributions to the coefficients $C_{2,3}$, whose presence is pointed out in [60], do not impact significantly for the range of SUSY parameters that we consider ($\tan\beta_S < 35$ and $|\theta_{\tilde{t}}| < \pi/10$).

The total contribution to C_1 can thus be written as

$$C_1^{tot}(M_W) = C_1^W(M_W) + C_1^{H^\pm}(M_W) + C_1^\chi(M_W) + C_1^{MI}(M_W)\ . \tag{21}$$

The explicit expressions for the various terms are:

$$C_1^W = C_1^{Wtt} + \left(\frac{V_{cq_1}V_{cq_2}^*}{V_{tq_1}V_{tq_2}^*}\right)^2 C_1^{Wcc} + 2\,\frac{V_{cq_1}V_{cq_2}^*}{V_{tq_1}V_{tq_2}^*}\,C_1^{Wtc}\ , \tag{22}$$

$$C_1^{H^\pm} = \frac{x_t^2}{4\ \tan^4\beta_S}\ Y_1(x_H,x_H,x_t,x_t) + \frac{x_t^2}{2\ \tan^2\beta_S}\ Y_1(1,x_H,x_t,x_t) - \frac{2x_t}{\tan^2\beta_S}\ Y_2(1,x_H,x_t,x_t)\ , \tag{23}$$

$$C_1^{\chi} = \sum_{i,j=1}^{2} \left| \tilde{V}_{i2} \frac{m_t \cos\theta_{\tilde{t}}}{\sqrt{2} M_W \sin\beta_S} - \sin\theta_{\tilde{t}} \tilde{V}_{i1}^* \right|^2 \times \left| \tilde{V}_{j2} \frac{m_t \cos\theta_{\tilde{t}}}{\sqrt{2} M_W \sin\beta_S} - \sin\theta_{\tilde{t}} \tilde{V}_{j1}^* \right|^2 \times Y_1(x_{\tilde{t}}, x_{\tilde{t}}, x_{\chi_i}, x_{\chi_j}) \,, \quad (24)$$

$$C_1^{MI} = \left| \frac{V_{ud}}{V_{td}} \right|^2 \sum_{i,j=1}^{2} \tilde{V}_{i1} \tilde{V}_{j1} \left(\tilde{V}_{i2} \frac{m_t \cos\theta_{\tilde{t}}}{\sqrt{2} M_W \sin\beta_S} - \sin\theta_{\tilde{t}} \tilde{V}_{i1}^* \right)^* \times \left(\tilde{V}_{j2} \frac{m_t \cos\theta_{\tilde{t}}}{\sqrt{2} M_W \sin\beta_S} - \sin\theta_{\tilde{t}} \tilde{V}_{j1}^* \right)^* \times Y_1^{MI}(x_{\tilde{q}}, x_{\tilde{t}}, x_{\chi_i}, x_{\chi_j}) \, \delta^2_{\tilde{u}_L \tilde{t}_2} \equiv \overline{C}_1^{MI} \, \delta^2_{\tilde{u}_L \tilde{t}_2} \quad (25)$$

where $C_1^{W\alpha\beta} = G(x_\alpha, x_\beta)$ and $x_\alpha = m_\alpha^2/M_W^2$. The contributions to C_1^{χ} and C_1^{MI} come from the Feynman diagrams shown in Fig. 1. The conventions we adopt for the chargino mass matrix, the exact definition of the stop mixing angle and the explicit expressions for the loop functions G, Y_1, Y_2 and Y_1^{MI} can be found in the appendices. Notice that, if we restrict to the B_d and B_s cases, one may neglect the terms C_1^{Wtc} and C_1^{Wcc} in (22) as they are suppressed by small CKM factors. In the K system, on the other hand, it is necessary to consider all the terms.

Equation (25) describes the impact of a non–zero mass insertion on the B_d *and* K systems. The corresponding contribution to the B_s system is obtained via the substitution

$$\left| \frac{V_{ud}}{V_{td}} \right|^2 \to \left| \frac{V_{us}}{V_{ts}} \right|^2 \,. \quad (26)$$

This implies that the impact of this diagram on the B_s system is reduced by a factor $|V_{us}V_{td}/V_{ts}|^2 \simeq 0.0016$ with respect to the B_d and K systems. Since, as we will show in the forthcoming analysis, C_1^{MI} is not likely to exceed by more than twice the SM contribution, it is clear that any effect in the B_s system from the mass insertion is completely negligible.

As already discussed in the introduction, the following structure of the SUSY contributions emerges in the class of model described above:

$$\begin{aligned} \Delta M_{B_s} : C_1^{Wtt} &\to C_1^{Wtt}(1+f) \\ \epsilon_K,\ \Delta M_{B_d},\ a_{\psi K_S} : C_1^{Wtt} &\to C_1^{Wtt}(1+f) + C_1^{MI} \\ &\equiv C_1^{Wtt}\,(1+f+g) \end{aligned}$$

where the parameters f and g represent normalized contributions from the MFV and MIA sectors, respectively,

$$f \equiv (C_1^{H^\pm} + C_1^{\chi})/C_1^{Wtt} \quad (27)$$

$$g \equiv g_R + i g_I \equiv \overline{C}_1^{MI} \delta^2_{\tilde{u}_L \tilde{t}_2}/C_1^{Wtt} \,. \quad (28)$$

The impact of the SUSY models on the observables we are interested in is then parametrized by three real parameters f, g_R and g_I. We recall here that in the limit $g \to 0$, the above parametrization reduces to the one given in [24, 25] for the minimal flavour violation and the MSSM cases (More generally, for all models in which the CKM matrix is the only flavour–changing structure). The absence of any CKM phase in (25) as well as in the definition of g reflects the definition of the mass insertion given in (11).

Note that f and g are functions of the SUSY parameters that enter in the computation of many other observables that are not directly related to CP violation. This implies that it is possible to look for processes that depend on the same SUSY inputs f and g. For example, the presence of non trivial experimental bounds on the $|\Delta B = 2|$, $\Delta Q = 0$ transitions can induce interesting correlations with the UT analysis. Likewise, the inclusive radiative decay $B \to X_s\gamma$ and $(g-2)_\mu$, the anomalous magnetic moment of the muon, are susceptible to supersymmetric contributions. On the other hand, it is necessary to search for observables that can put constraints on the insertion $\delta_{\tilde{u}_L \tilde{t}_2}$. In this context, the transitions $b \to d\gamma$, $B^0 \to \rho^0\gamma$ and $B^\pm \to \rho^\pm\gamma$ are obvious places to look for $\delta_{\tilde{u}_L \tilde{t}_2}$–related effects.

Concerning now the $(g-2)_\mu$ constraint, we recall that the Brookhaven Muon $(g-2)$-collaboration has recently measured with improved precision the anomalous magnetic moment of the positive muon. The present world average for this quantity is [44]

$$a_{\mu^+}(\text{exp}) = 116592023(15) \times 10^{-10} \,. \quad (29)$$

The contribution to a_{μ^+} in the SM arises from the QED and electroweak corrections and from the hadronic contribution which includes both the vacuum polarization and light by light scattering [61]. The error in the SM estimate is dominated by the hadronic contribution to a_{μ^+} and is obtained from $\sigma(e^+e^- \to \text{hadrons})$ via a dispersion relation and perturbative QCD. The light-by-light hadronic contribution is, however, completely theory-driven. Several competing estimates of $a_{\mu^+}^{had}$ exist in the literature, reviewed recently in [62]. We briefly discuss a couple of representative estimates here.

In order to minimize the experimental errors in the low-s region, Davier and Höcker supplemented the $e^+e^- \to \pi^+\pi^-$ cross section using data from tau decays. Using isospin symmetry they estimate [63]

$$a_{\mu^+}^{had} = (692.4 \pm 6.2) \times 10^{-10} \,. \quad (30)$$

An updated value of $a_{\mu^+}^{had}$ using earlier estimates of Eidelman and Jegerlehner [64] supplemented by the recent data from CMD and BES collaborations yields [65]

$$a_{\mu^+}^{had} = (698.75 \pm 11.11) \times 10^{-10} \,. \quad (31)$$

Alternatively, calculating the Adler function from e^+e^- data and perturbative QCD for the tail (above 11 GeV) and calculating the shift in the electromagnetic fine structure constant $\Delta\alpha^{had}$ in the Euclidean region, Jegerlehner quotes [65]

$$a_{\mu^+}^{had} = (697.4 \pm 10.45) \times 10^{-10} \,. \quad (32)$$

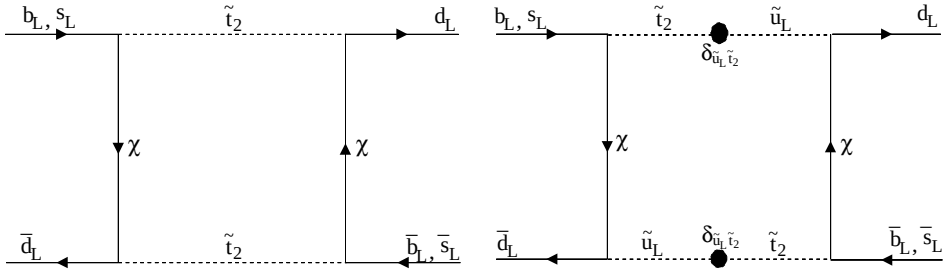

Fig. 1. Feynman diagrams contributing to C_1^{χ} and C_1^{MI} respectively. The bubble represents the mass insertion $\delta_{\tilde{u}_L\tilde{t}_2}$

These estimates are quite compatible with each other, though the errors in (31) and (32) are larger than in (30). Adopting the theoretical estimate from Davier and Höcker [63], one gets

$$a_{\mu^+}(\mathrm{SM}) = 11659163(7)\times 10^{-10}\ , \tag{33}$$

yielding

$$\delta a_{\mu^+} \equiv a_{\mu^+}(\exp) - a_{\mu^+}(\mathrm{SM}) = +43(16)\times 10^{-10}, \tag{34}$$

which is a 2.6 σ deviation from the SM. Using, however, the estimate from Jegerlehner in (32), gives

$$\delta a_{\mu^+} = +37(18)\times 10^{-10}, \tag{35}$$

which amounts to about 2 σ deviation from the SM. Estimates of δa_{μ^+} ($= 33(17)\times 10^{-10}$) by Narison [66] are similar. Thus, on the face-value, there exists a 2 to 2.6 σ discrepancy between the current experiments on $(g-2)_\mu$ and SM-estimates.

In SUSY theories, a_{μ^+} receives contributions via vertex diagrams with χ^0–$\tilde{\mu}$ and $\chi^{\pm}$–$\tilde{\nu}$ loops [61,67–78]. The chargino diagram strongly dominates over almost all the parameter space. The chargino contribution is [67] (see also [68] for a discussion on CP violating phases):

$$\delta a_{\mu^+}^{\chi\tilde{\nu}} = \frac{g_2^2}{8\pi^2}\frac{M_\mu^2}{M_{\tilde{\nu}}^2}\sum_{i=1}^{2}\left\{\left[\frac{M_\mu^2\,\mathrm{Re}\,(\tilde{U}_{i2}^2)}{2M_W^2\cos^2\beta_S} + \mathrm{Re}\,(\tilde{V}_{i1}^2)\right]F_1(x_i) - \frac{M_{\chi_i}\mathrm{Re}(\tilde{U}_{i2}\tilde{V}_{i1})}{\sqrt{2}M_W\cos\beta}F_3(x_i)\right\}\ , \tag{36}$$

where $x_i = M_{\chi_i}^2/M_{\tilde{\nu}}^2$ and the loop functions F_1 and F_3 are given in the appendices. (36) is dominated by the last term in curly brackets whose sign is determined by $\mathrm{sign}[\mathrm{Re}(\tilde{U}_{12}\tilde{V}_{11})] = -\mathrm{sign}[\mathrm{Re}(\mu)]$ (note that we have $M_{\chi_1} < M_{\chi_2}$). Taking into account that the Brookhaven experiment implies $\delta a_{\mu^+} > 0$ at 2 to 2.6 σ, it is clear that the $\mu > 0$ region is currently favoured.

Finally let us focus on $b \to d\gamma$ decays. To the best of our knowledge, there is no direct limit on the inclusive decay $b \to d\gamma$. The present experimental upper limits on some of the exclusive branching ratios are

$$\mathcal{B}(B^0 \to \rho^0\gamma) < 0.56\times 10^{-5} \quad (90\%\ \mathrm{C.L.})[45]\ , \tag{37}$$
$$\mathcal{B}(B^+ \to \rho^+\gamma) < 1.3\times 10^{-5} \quad (90\%\ \mathrm{C.L.})[79]\ , \tag{38}$$
$$R(\rho\gamma/K^*\gamma) \equiv \mathcal{B}(B\to\rho\gamma)/\mathcal{B}(B\to K^*\gamma) < 0.28 \quad (90\%\ \mathrm{C.L.})[45]\ . \tag{39}$$

In the numerical analysis we will use only the last constraint since the ratio of branching ratios is theoretically cleaner as only the ratio of the form factors is involved, which is calculable more reliably. Concentrating on the neutral B-decays, the LO expression for $R(\rho\gamma/K^*\gamma)$ is [80,81]

$$R(\rho\gamma/K^*\gamma) = \frac{2\mathcal{B}(B^0\to\rho^0(770)\gamma)}{\mathcal{B}(B\to K^*\gamma)} = \left|\frac{V_{td}}{V_{ts}}\right|^2\left(\frac{M_B^2 - M_\rho^2}{M_B^2 - M_{K^*}^2}\right)^3\xi\left|\frac{C_7^d(m_b)}{C_7^s(m_b)}\right|^2\ , \tag{40}$$

where

$$\xi = \left|\frac{F_1^{B^0\to\rho^0}}{F_1^{B^0\to K^{*0}}}\right|^2\ , \tag{41}$$

with $F_1^{B^0\to\rho^0,K^{*0}}$ being the form factors involving the magnetic moment (short–distance) transition; $M_B = 5.2794$ GeV, $M_{K^*} = 0.8917$ GeV, $M_{\rho^0} = 0.7693$ GeV and $\xi = 0.58$ [80]. $C_7^{(d,s)}(m_b)$ is the Wilson coefficient of the magnetic moment operator for the transition $b\to(d,s)$ computed in the leading order approximation. Note that the annihilation contribution (which is estimated at about 25 % in $B^\pm \to \rho^\pm\gamma$ [82,83]) is suppressed due to the unfavourable colour factor and the electric charge of the d–quark in B^0, and ignored here. In the SM, these two Wilson coefficients coincide while, in the SUSY model we consider, they differ because of the effect of the insertion $\delta_{\tilde{u}_L\tilde{t}_2}$:

$$C_7^s(M_W) = C_7^W(M_W) + C_7^{H^\pm}(M_W) + C_7^{\chi}(M_W)\ , \tag{42}$$
$$C_7^d(M_W) = C_7^s(M_W) + C_7^{MI}(M_W)\ . \tag{43}$$

where C_7^W, $C_7^{H^\pm}$ and C_7^{χ} are, respectively, the SM, the charged Higgs and the chargino contributions and their explicit expressions can be found for instance in [57,23]. The explicit expression for the mass insertion contribution is

$$C_7^{MI}(M_W) = \left|\frac{V_{ud}}{V_{td}}\right|\sum_{i=1}^{2}\frac{M_{\tilde{q}}M_{\tilde{t}_2}M_W}{6M_{\chi_i}^3}\tilde{V}_{i1} \times\left\{\left(\frac{\tilde{V}_{i2}^* m_t\cos\theta_{\tilde{t}}}{\sqrt{2}M_W\sin\beta_S} - \tilde{V}_{i1}^*\sin\theta_{\tilde{t}}\right) \times\frac{M_W}{M_{\chi_i}}f_1^{MI}(x_{\tilde{t}_2\chi_i}, x_{\tilde{q}\chi_i})\right.$$

$$+\frac{\sqrt{2}\tilde{U}_{i2}\sin\theta_{\tilde{t}}}{\cos\beta_S} f_2^{MI}(x_{\tilde{t}_2\chi_i}, x_{\tilde{q}\chi_i})\Bigg\}\delta_{\tilde{u}_L\tilde{t}_2} \quad (44)$$

$$\equiv \overline{C}_7^{MI}\delta_{\tilde{u}_L\tilde{t}_2} \quad (45)$$

where the loop functions f_1^{MI} and f_2^{MI} are given in Appendix B. Using (43) and (45) it is possible to rewrite the ratio $R(\rho\gamma/K^*\gamma)$ in the following way:

$$R(\rho\gamma/K^*\gamma) = R^{SM}\left|1+\delta_{\tilde{u}_L\tilde{t}_2}\frac{\eta^{\frac{16}{23}}\overline{C}_7^{MI}}{C_7^s(m_b)}\right|^2 \quad (46)$$

in which $\overline{C}_7^{MI}$ and $C_7^s(m_b)$ are both real, $\eta^{\frac{16}{23}}$ is a QCD factor numerically equal to 0.66 and we have abbreviated $R(\rho\gamma/K^*\gamma)^{SM}$ by R^{SM} for ease of writing.

4 Numerical analysis of SUSY Contributions

In this section we study the correlations between the possible values of the parameters f and g as well as the numerical impact of $b\to s\gamma$, $\delta_{a_{\mu^+}}$ and $b\to d\gamma$ with the following experimental constraints

$$\begin{aligned}
&2.41\times10^{-4}\le\mathcal{B}(B\to X_s\gamma)\le 4.02\times10^{-4} \quad (95\%\ \text{C.L.})\\
&10\times10^{-10}\le\delta a_{\mu^+}\le 74\times10^{-10} \quad (95\%\ \text{C.L.})\\
&R(\rho\gamma/K^*\gamma)\le 0.28 \quad (90\%\ \text{C.L.})
\end{aligned} \quad (47)$$

where we have used the estimates of $\delta a_{\mu^+}(\text{SM})$ from (30). We perform the numerical analysis by means of high density scatter plots varying the SUSY input parameters over the following ranges:

$$\left\{\begin{array}{rcl}
\mu &=& (100\div1000)\ \text{GeV}\,,\\
M_2 &=& (100\div1000)\ \text{GeV}\,,\\
\tan\beta_S &=& 3\div35\,,\\
M_{H^\pm} &=& (100\div1000)\ \text{GeV}\,,\\
M_{\tilde{t}_2} &=& (100\div600)\ \text{GeV}\,,\\
\theta_{\tilde{t}} &=& -0.3\div0.3\,.
\end{array}\right. \quad (48)$$

Notice that, according to the discussion of the previous section, we restrict the scatter plot to positive μ values only. Negative values are strongly disfavoured both by the $\delta a_{\mu^+}\ge 0$ bound and by the $b\to s\gamma$ branching ratio. In fact, it is possible to show that if μ is negative, the chargino contributions to $b\to s\gamma$ tend to interfere constructively with the SM and the charged Higgs ones. In order not to exceed the experimental upper limit, a quite heavy SUSY spectrum is thus required. In such a situation, high f and g values are quite unlikely.

In Fig. 2 we plot the points in the $(f,|g|)$ plane that survive the $b\to s\gamma$, δa_{μ^+} and $b\to d\gamma$ constraints. Scanning over the parameters given in (48) we find that the constraints in (47) restrict f and $|g|$ to lie essentially in the range $f<0.4$, $|g|<2.0$. We also find that the sign of $\overline{C}_1^{MI}/C_1^{Wtt}$ is positive over all the SUSY parameter space that we scanned.

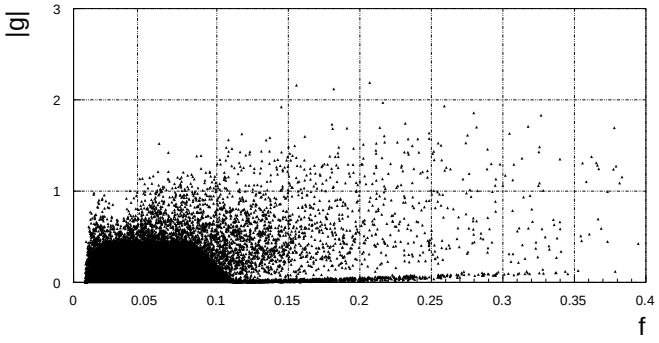

Fig. 2. Allowed points in the $(f,|g|)$ plane. The ranges of the supersymmetric parameters and the constraints from $b\to s\gamma$, δa_{μ^+} and $b\to d\gamma$ that we impose are given in (48) and (47) respectively

The impact of δa_{μ^+} on our analysis is not very strong, once we limit the scanning to the $\mu>0$ region only. Moreover, as follows from (36), the size of the chargino contribution to δa_{μ^+} is controlled by the mass of the muon sneutrino. In our framework, $m_{\tilde{\nu}}$ is a free parameter and we have imposed the lower bound $\delta a_{\mu^+}\ge 10\times10^{-10}$ in the loosest possible way by choosing $m_{\tilde{\nu}}=100$ GeV (a value that is reasonably safe against direct search constraints). On the other hand, we can not reject points which give a too large contribution to δa_{μ^+} because a large enough sneutrino mass can always suppress the SUSY diagram and reduce δa_{μ^+} to a value smaller than 74×10^{-10}. Notice that, if $m_{\tilde{\nu}}\ge 300$ GeV, all the points that we consider do satisfy the upper bound: in order to obtain larger contributions it is necessary to impose a very light sneutrino mass. Only models in which the squark and the slepton mass spectra depend on the same inputs will be able to fully exploit the correlation between the anomalous magnetic moment of the muon and observables related to B physics.

The impact of the $b\to d\gamma$ constraint is taken into account by imposing the following upper bound on the mass insertion:

$$\left|\delta_{\tilde{u}_L\tilde{t}_2}\right| < \left(\sqrt{\frac{0.28}{R^{SM}}}-1\right)\left|\frac{C_7^s(m_b)}{\eta^{\frac{16}{23}}\overline{C}_7^{MI}}\right| . \quad (49)$$

Again, we find that with the current experimental bound $R(\rho\gamma/K^*\gamma)<0.28$, most of the otherwise allowed $(f,|g|)$ region survives. This situation will change with improved limits (or measurements of $R(\rho\gamma/K^*\gamma)$).

In Fig. 3 we perform the same analysis presented in Fig. 2 but we allow only for points that give a positive sign for the Wilson coefficient C_7^s computed in the LO approximation. The issue whether it is possible or not to change the sign of C_7^s depends on the model and has been long debated in the literature. In particular, this sign strongly characterizes the behaviour of the forward–backward asymmetry and of the dilepton invariant mass in $b\to s\ell^+\ell^-$ transitions, as well as the sign of the isospin violating ratio Δ (see below) and of the CP-violating asymmetry in the radiative decays $B\to\rho\gamma$ [81]. We use C_7^{LO} for calculating the CP-asymmetry in $B\to\rho\gamma$. The quan-

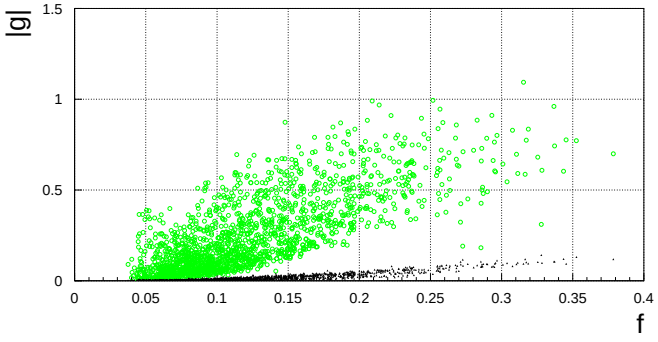

Fig. 3. Allowed points in the $(f, |g|)$ plane that are compatible with a positive value of the Wilson coefficient C_7. The empty circles satisfy the $b \to s\gamma$ and δa_{μ^+} constraints. The impact of imposing in addition the upper bound on the $b \to d\gamma$ transition is represented by the black dots

tity Δ in the NLO approximation requires the Wilson coefficient C_7^{NLO}. However, as shown in [81], Δ is stable against NLO vertex corrections. Recently, also the so–called hard spectator corrections have been calculated to $O(\alpha_s)$ in $B \to \rho\gamma$ [84,85] with the result that Δ is stable also against these corrections. We refer to [81,86,87,55,88] for a comprehensive review of the positive C_7 phenomenology. In Fig. 3, open circles represent points that satisfy the $b \to s\gamma$ and δa_{μ^+} constraints. The black dots show what happens when the experimental bound $R(\rho\gamma/K^*\gamma) < 0.28$ is imposed. In implementing this constraint we use (49). If for a given point $\delta^{\rm lim}$ turns out to be smaller than 1, we plot $|g|_{\delta=\delta^{\rm lim}}$, otherwise we set $\delta = 1$. It is important to note that the dependence of C_7^{MI} and C_1^{MI} on the mass insertion is, respectively, linear and quadratic. From Fig. 3 one sees that all the points that are compatible with a positive C_7 provide, indeed, a too large contribution to $b \to d\gamma$, and hence are effectively removed by the cut on $R(\rho\gamma/K^*\gamma)$. This result is quite reasonable because, in order to change the sign of C_7, a large positive chargino contribution is needed: since C_7^{χ} and $\overline{C}_7^{MI}$ depend on the same input parameters we expect their magnitude to be closely correlated. In Fig. 4, we show explicitly the correlation between $C_7^s(m_b)$ and $\overline{C}_7^{MI}(m_b) \equiv \eta^{\frac{16}{23}}\overline{C}_7^{MI}(M_W)$ in both the negative and positive C_7^s allowed regions. In the second plot, in particular, $|C_7^{MI}(m_b)|$ turns out to be greater than one for all the points: this implies that the mass insertion constraint is always non trivial. The strong bound shown in Fig. 3 is obtained by taking into account that g depends quadratically on $\delta_{\tilde{u}_L\tilde{t}_2}$. The conclusion is that if $C_7^s > 0$ is experimentally established, our analysis implies strong constraints on the quantity $|g|$ from $b \to d\gamma$ decays, permitting only small deviations from the MFV-value: $|g| = 0$.

5 Unitarity triangle analysis

In Sect. 3 we have shown that the impact of this class of SUSY models on observables related to the unitarity triangle (UT) can be parameterized by two real parameters and by one phase (see (9) and (10)). In this section we analyze the implications of this parametrization on the standard analysis of the UT. As usual we use the Wolfenstein parametrization [36] of the CKM matrix in terms of λ, A, ρ and η:

$$V = \begin{pmatrix} 1-\frac{\lambda^2}{2} & \lambda & A\lambda^3(\rho - i\eta) \\ -\lambda & 1-\frac{\lambda^2}{2} & A\lambda^2 \\ A\lambda^3(1-\rho-i\eta) & -A\lambda^2 & 1 \end{pmatrix} . \quad (50)$$

In the following analysis we extend this parametrization beyond the leading order in λ; as a consequence it is necessary to study the unitarity triangle in the plane $(\bar{\rho}, \bar{\eta})$ where $\bar{\rho} = \rho\,(1 - \lambda^2/2)$ and $\bar{\eta} = \eta\,(1 - \lambda^2/2)$ [89].

Let us collect the relevant formulae for ϵ_K, $\Delta M_{B_{(d,s)}}$ and $a_{\psi K_S}$ as functions of f, g and $\delta_{\tilde{c}_L\tilde{t}_2}$:

$$\epsilon_K = -\frac{G_F^2 f_K^2 \hat{B}_K M_K M_W^2}{12\sqrt{2}\pi^2 \Delta M_K} \mathrm{Im}\Big\{\lambda_c^{*2}\eta_{cc} C_1^{Wcc} + 2\lambda_c^*\lambda_t^*\eta_{tc} C_1^{Wtc} + \lambda_t^{*2}\eta_{tt} C_1^{Wtt}(1+f+g)\Big\} e^{\frac{i\pi}{4}} , \quad (51)$$

$$\Delta M_{B_d} = -\frac{G_F^2}{6\pi^2}\eta_B M_{B_d} f_{B_d}^2 \hat{B}_{B_d} M_W^2 |V_{tb}V_{td}^*|^2 \times C_1^{Wtt}|1+f+g| , \quad (52)$$

$$\Delta M_{B_s} = -\frac{G_F^2}{6\pi^2}\eta_B M_{B_s} f_{B_s}^2 \hat{B}_{B_s} M_W^2 |V_{tb}V_{ts}^*|^2 \times C_1^{Wtt}(1+f) , \quad (53)$$

$$a_{\psi K_S} = \sin 2(\beta + \theta_d) \quad (54)$$

where $\lambda_q = V_{qd}V_{qs}^*$, $\theta_d = \frac{1}{2}\arg(1+f+g)$, β denotes the phase of V_{td}^* and from (50) it follows

$$\sin 2\beta = \frac{2\bar{\eta}(1-\bar{\rho})}{(1-\bar{\rho}^2)+\bar{\eta}^2} . \quad (55)$$

The quantities η_{tt}, η_{cc}, η_{cc}, and η_B are NLO QCD corrections. Their values together with those of the other parameters are collected in Table 1.

Table 1. Parameters used in the UT-fits

Parameter	Value
η_{tt}	0.57 [90]
η_{cc}	1.38 ± 0.53 [91]
η_{tc}	0.47 ± 0.04 [92]
$\hat{B}_K$	0.94 ± 0.15 [93,94]
η_B	0.55 [90]
$f_{B_d}\sqrt{\hat{B}_{B_d}}$	230 ± 40 MeV [93–95]
$\xi_s = \frac{f_{B_s}\sqrt{\hat{B}_{B_s}}}{f_{B_d}\sqrt{\hat{B}_{B_d}}}$	1.16 ± 0.05 [96]

Our first step is to investigate the regions of the parameter space spanned by f, g_R and g_I that are allowed by the present experimental data. The procedure consists in writing the χ^2 of the selected observables and in accepting only values of f and g which satisfy the condition

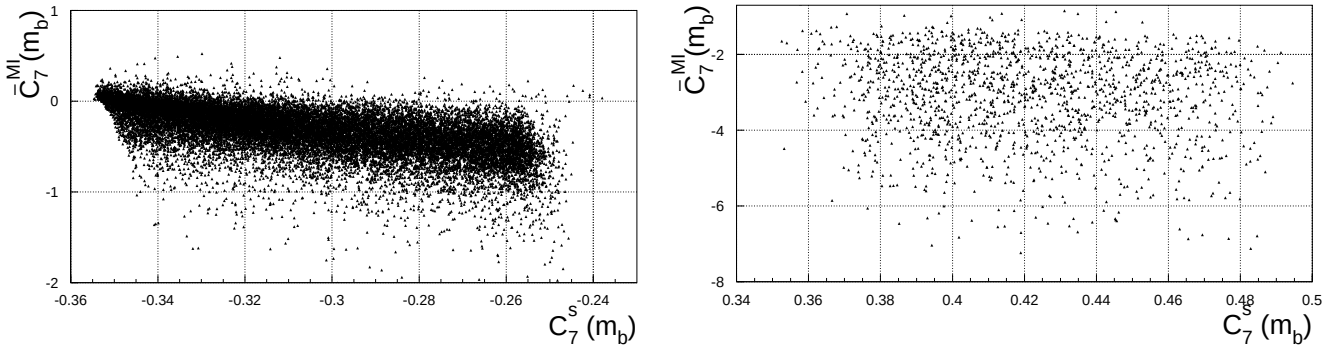

Fig. 4. Correlation between the SUSY contributions to $C_7^s(m_b)$ and $\overline{C}_7^{MI}(m_b)$. The plots correspond to the negative (left figure) and positive (right figure) solutions for $C_7^s(m_b)$ allowed by the experimental bounds on $\mathcal{B}(B \to X_s\gamma)$. Note that $C_7^d(m_b) = C_7^s(m_b) + \overline{C}_7^{MI}(m_b)\,\delta_{\tilde{u}_L\tilde{t}_2}$

$\min_{\rho,\eta}(\chi^2) \leq 2$. In the computation of χ^2 we use the following input

$$\epsilon_K = (2.271 \pm 0.017)\ 10^{-3}[\text{PDG [11]}], \quad (56)$$

$$\Delta M_{B_d} = 0.484 \pm 0.010\ \text{ps}^{-1}[\text{HFWG [10]}], \quad (57)$$

$$\left|\frac{V_{ub}}{V_{cb}}\right| = 0.090 \pm 0.025[\text{PDG [11]}], \quad (58)$$

$$a_{\psi K_s} = 0.79 \pm 0.12\ . \quad (59)$$

The value quoted above for ΔM_{B_d} is the present world average of experiments on B - $\bar{B}$ mixings, including the recent BABAR [8] and BELLE [9] measurements. We introduce the experimental data on ΔM_{B_s} in calculating the chi–squared (χ^2) using the so–called amplitude method [97]. The prescription consists in adding to the χ^2 the term $\chi^2_{\Delta M_{B_s}} = (1-\mathcal{A})^2/\sigma^2_{\mathcal{A}}$ where $\mathcal{A}$ is the amplitude of the $(B_s - \bar{B}_s)$ oscillation, given by $(1 \pm \mathcal{A}\cos\Delta M_{B_s} t)$, and $\sigma_{\mathcal{A}}$ is the corresponding error. Both $\mathcal{A}$ and $\sigma_{\mathcal{A}}$ are functions of ΔM_{B_s}. Notice that using this method, the statistical interpretation of the value of the χ^2 in its minimum is preserved. In [98], the authors include the ΔM_{B_s} data using an alternative procedure. They consider a log–likelihood function referenced to $\Delta M_{B_s} = \infty$ and add the term $\Delta \log L^{\infty} = (1/2 - \mathcal{A})/\sigma_{\mathcal{A}}$ to the χ^2. In this way the significance of the data is increased. Notice that, in order to interpret the output of this method in terms of confidence levels it is necessary to perform a monte–carlo based analysis [99]. Since we are interested in the statistical meaning of the minimum of the χ^2, we prefer to use the standard amplitude analysis.

We present the output of this analysis in Fig. 5 a. For each contour we fix the value of f and we require the χ^2_{min} to be less than 2. Since, as can be seen in Fig. 2, f is always smaller than 0.4, we restrict the analysis to $f = 0$, 0.2 and 0.4. Moreover, for each of these values, we require $|g|$ not to exceed the upper limit which, according to the analysis of the SUSY contributions presented in Fig. 2, we set respectively to 1, 2 and 1.5. The equation $\sin 2(\beta + \theta_d) = a_{\psi K_S}$ has two solutions (mod π) in which $(\beta + \theta_d)$ lies in the ranges $[0, \pi/4]$ and $[\pi/4, \pi/2]$ respectively. This implies that, given a value of f, we expect two distinct allowed regions in the (g_R, g_I) plane, that we call respectively small and large angle solutions, characterized by $\beta + \theta_d < \pi/4$ (i.e. $\theta_d \simeq O(0.1)$ and $\beta + \theta_d > \pi/4$ (i.e. $\theta_d \simeq O(1)$). These two regions have some overlap since in the limit $a_{\psi K_S} = 1$ (which is allowed at 90% C.L.) the two solutions coincide. We find that, once the upper bound on $|g|$ is imposed, only a small part of the $f = 0.2$ and a tiny corner of the $f = 0.4$ large angle solution survive. Improvements in the experimental determination of the $B \to X_s\gamma$ and $B \to \rho\gamma$ branching ratios as well as more stringent lower bounds on the SUSY spectrum will have a strong impact on the allowed $|g|$ values. On the other hand, more precise measurements of $|V_{ub}/V_{cb}|$, $a_{\psi K_S}$, ΔM_{B_s} and progress in the determination of the relevant hadronic parameters, will contribute to reduce sizably the size of the allowed (g_R, g_I) regions. In view of these considerations, we expect the large angle ($\theta_d \simeq O(1)$) solution is less likely to survive in future and we will concentrate in the following on the small angle scenario, i.e., $\theta_d \simeq O(0.1)$.

It is interesting to note that the amplitude method, that is conservatively used to set the constraint $\Delta M_{B_s} > 14.9\ \text{ps}^{-1}$ at 95% C.L., also yields a 2.5 σ signal for oscillations around $\Delta M_{B_s} = 17.7\ \text{ps}^{-1}$. This would–be measurement is equivalent to a determination of the ratio $\Delta M_{B_s}/\Delta M_{B_d}$ which in turn depends on the precisely computed hadronic parameter ξ_s: its impact on the unitarity triangle is thus expected to be quite significant [15]. In Fig. 5 b we assume this signal to be a measurement with $\Delta M_{B_s} = 17.7 \pm 1.4\ \text{ps}^{-1}$ in order to explore its implications on the previous analysis. The effect of the assumed value of ΔM_{B_s} is to reduce the $g_R, g_I > 0$ allowed regions; moreover, its impact is stronger the higher is the value of f. Note, in particular, that, with the assumed value of ΔM_{B_s}, the $f = 0.4$ contour almost disappeared. This happens because the experimentally favoured high values of $a_{\psi K_S}$ tend to sharpen the mismatch between the ΔM_{B_d} and $\Delta M_{B_s}/\Delta M_{B_d}$ constraints (which is due to a non–zero value of f).

Before concluding this section we would like to show the impact of the Extended-MFV model considered in this paper on the profile of the unitarity triangle in the $(\bar{\rho}, \bar{\eta})$ plane, and the corresponding profiles in the SM and MFV models. In Fig. 6, the solid contour corresponds

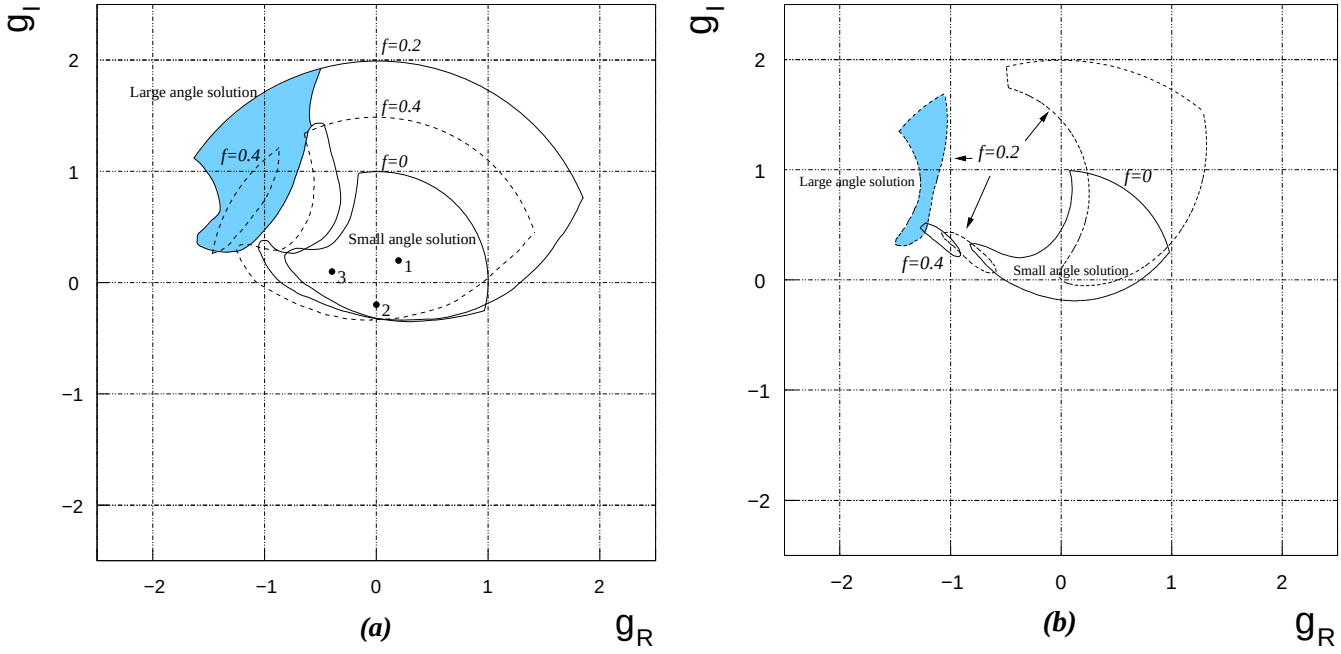

Fig. 5. a Region of the (g_R, g_I) plane for which $\min_{\rho,\eta}(\chi^2) \leq 2$ from the CKM-UT fits. The ΔM_{B_s} constraint is taken into account using the amplitude method. The contours correspond to f = 0, 0.2 and 0.4 and the constraints on $|g|$, coming from Fig. 2, are $|g| \leq 1$, 2 and 1.5 respectively. The shaded areas correspond to a solution with $\theta+\beta > 45^\circ$ and are allowed for $f = 0.2$ and $f = 0.4$. The three dots are representative points that we use to illustrate the impact of the parametrization we propose on the unitarity triangle. **b** The same as in **a**, but interpreting the 2.5 σ enhancement in the amplitude as $\Delta M_{B_s} = 17.7 \pm 1.4$ ps^{-1}

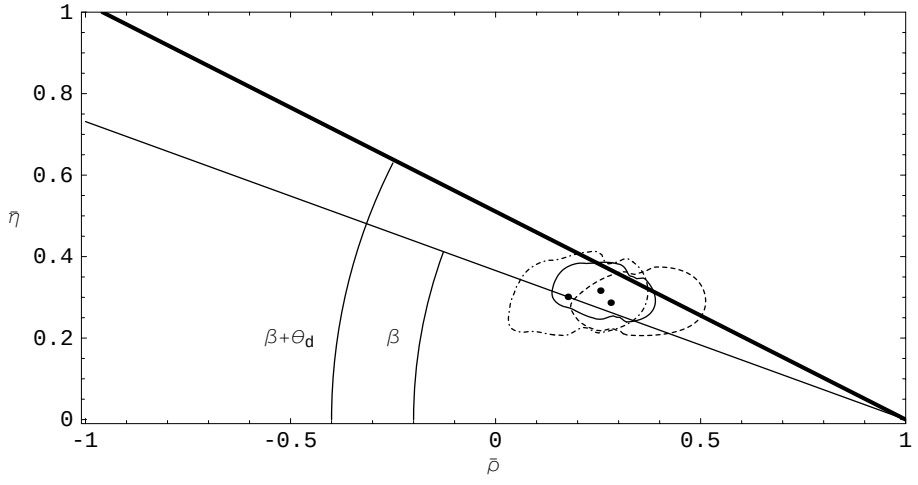

Fig. 6. Allowed 95 % $C.L.$ contours in the $(\bar\rho, \bar\eta)$ plane. The solid contour corresponds to the SM case, the dashed contour to the Minimal Flavour Violation case with ($f = 0.4$, $g = 0$) and the dashed–dotted contour to the Extended-MFV model discussed in the text ($f = 0$, $g_R = -0.2$, $g_I = 0.2$)

to the SM 95% C.L., the dashed one to a typical MFV case ($f = 0.4$, $g = 0$) and the dotted–dashed one to an allowed point in the Extended-MFV model ($f = 0$, $g_R = -0.2$ and $g_I = 0.2$). The representative point that we consider survives all the experimental constraints examined in the previous section. Using the values of $\bar\rho$ and $\bar\eta$ that correspond to the central value of the fit, we obtain the following results for the various observables: $|V_{ub}/V_{cb}| = 0.079$, $\epsilon_K = 2.27 \times 10^{-3}$, $\Delta M_{B_d} = 0.484$ ps^{-1}, $\Delta M_{B_s} = 20.7$ ps^{-1} and $a_{\psi K_S} = 0.81$. If $|g|$ is sufficiently large, θ_d can be regarded as an essentially free parameter and the fit will choose the value that gives the best agreement with the experimental measurement. In Fig. 7 we plot the CP asymmetry $a_{\psi K_S}$ as a function of $\arg \delta_{\tilde u_L \tilde t_2}$ (expressed in degrees). The light and dark shaded bands correspond, respectively, to the SM and the experimental 1 σ allowed regions. The solid line is drawn for $f = 0$ and $|g| = 0.28$. The experimental band favours $\arg \delta_{\tilde u_L \tilde t_2}$ in the range $[0^\circ, 100^\circ]$. Employing the explicit dependence

$$\theta_d = \frac{1}{2} \arg(1 + f + |g| e^{2i \arg \delta_{\tilde u_L \tilde t_2}}) \pmod \pi , \qquad (60)$$

the above phase interval is translated into $-3^\circ < \theta_d < 8^\circ$, for the assumed values of $|g|$ and f, which is a typical range for θ_d for the small angle solution with the current values of $a_{\psi K_S}$.

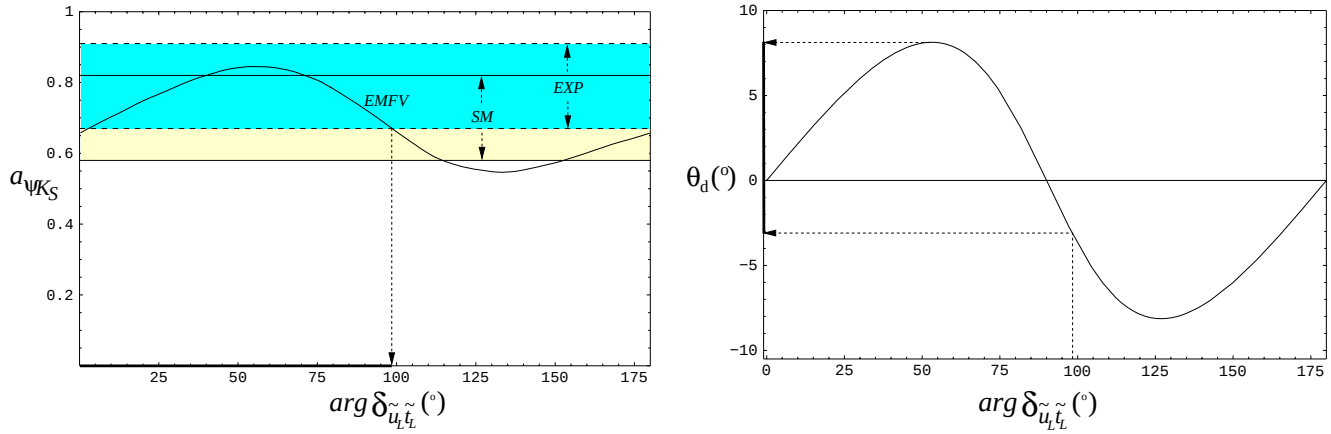

Fig. 7. The CP asymmetry $a_{\psi K_S}$ as a function of $\arg\delta_{\tilde{u}_L\tilde{t}_2}$ expressed in degrees. The solid curve corresponds to the Extended-MFV model ($f=0,\ |g|=0.28$). The light and dark shaded bands correspond, respectively, to the allowed 1 σ region in the SM ($0.58 \le a_{\psi K_S} \le 0.82$) and the current 1 σ experimental band ($0.67 \le a_{\psi K_S} \le 0.91$). The plot on the right shows the correlation between $\arg\delta_{\tilde{u}_L\tilde{t}_2}$ and the angle θ_d: $\theta_d = \frac{1}{2}\arg(1+f+|g|e^{2i\arg\delta_{\tilde{u}_L\tilde{t}_2}})$, (mod π). The experimentally allowed region favours $0^\circ < \arg\delta_{\tilde{u}_L\tilde{t}_2} < 100^\circ$ that translates into $-3^\circ < \theta_d < 8^\circ$

In order to illustrate the possible different impact of this parametrization on the unitarity triangle analysis, we focus on the $f=0$ case and choose three extremal points inside the allowed region in the plane (g_R, g_I). We concentrate on the small angle scenario. In Fig. 8 we plot the 95% C.L. contours in the $(\bar\rho,\bar\eta)$ plane that correspond to the points we explicitely show in Fig. 5 a. We summarize in Table 2 the central values of $|V_{ub}/V_{cb}|$, ΔM_{B_s}, the CP asymmetry $a_{\psi K_S}$, the inner angles α and γ of the unitarity triangle computed for the different contours. Contour 1 is drawn for positive g_I and θ_d is consequently positive. This implies that $a_{\psi K_S}$ is expected to be larger than in the SM. The CP asymmetry and $|V_{ub}/V_{cb}|$ are very close to their world averages while the angle γ is smaller than γ^{SM}. In contour 2 the phase θ_d is negative and the CP asymmetry is thus predicted to be lower than the experimental central value and still $\gamma < \gamma^{SM}$. Contour 3 is drawn for $g = -0.4 + 0.1i$ and is particularly interesting since it corresponds to a solution in which $a_{\psi K_S}$ is larger than in the SM and the Wolfenstein parameter $\bar\rho$ is negative, i.e. $\bar\rho < 0$, implying a value of the inner angle γ in the domain $\pi/2 < \gamma < \pi$. This is in contrast with the SM–based analyses which currently yield $\gamma < \pi/2$ at 2 standard deviations [12–19] and with the other solutions shown in Fig. 8. We note that analyses [48,49] of the measured two–body non–leptonic decays $B \to \pi\pi$ and $B \to K\pi$ have a tendency to yield a value of γ which lies in the range $\gamma > \pi/2$ (restricting to the solutions with $\bar\eta > 0$). While present data, and more importantly the non–perturbative uncertainties in the underlying theoretical framework do not allow to draw quantitative conclusions at present, this may change in future. In case experimental and theoretical progress in exclusive decays force a value of γ in the domain $\pi/2 < \gamma < \pi$, the extended–MFV model discussed here would be greatly constrained and assume the role of a viable candidate to the SM.

In Fig. 9 and Table 3 we show the consequences, on the analysis described above, of reducing the error on the CKM ratio $|V_{ub}/V_{cb}|$ by a factor of 2. The value $|V_{ub}/V_{cb}| = 0.090 \pm 0.013$, used by us to illustrate the improved constraint on the CKM unitarity triangle, is obtained from the inclusive measurement of $|V_{cb}|$ from CLEO [41] and LEP [100], yielding $|V_{cb}| = (40.57 \pm 1.21)\times 10^{-3}$, and the average of the currently measured values of $|V_{ub}|$ by the CLEO [101] and LEP [100] groups, yielding $|V_{ub}| = (3.64 \pm 0.46)\times 10^{-3}$. Note that the reduced error on $|V_{ub}/V_{cb}|$ does not affect sizably the existence of the $\bar\rho < 0$ solution in the extended–MFV model shown here.

Table 2. Central values of the CKM ratio $|V_{ub}/V_{cb}|$, the $B_s - \bar B_s$ mass difference ΔM_{B_s}, the CP asymmetry $a_{\psi K_S}$ and the inner angles α and γ of the unitarity triangle for the contours in the extended–MFV model plotted in Fig. 8. The (g_R, g_I) values for the contours are also indicated

Contour	g_R	g_I	$\lvert V_{ub}/V_{cb}\rvert$	ΔM_{B_s}	$a_{\psi K_S}$	α	γ
1	0.2	0.2	0.094	20 ps^{-1}	0.78	119°	40°
2	0.0	−0.2	0.110	20 ps^{-1}	0.71	101°	51°
3	−0.4	0.1	0.081	17 ps^{-1}	0.73	64°	98°

Table 3. The same as in Table 2. The error on $|V_{ub}/V_{cb}|$ is reduced by a factor of 2

Contour	g_R	g_I	$\lvert V_{ub}/V_{cb}\rvert$	ΔM_{B_s}	$a_{\psi K_S}$	α	γ
1	0.2	0.2	0.092	20 ps^{-1}	0.77	120°	40°
2	0.0	−0.2	0.102	20 ps^{-1}	0.65	101°	53°
3	−0.4	0.1	0.084	17 ps^{-1}	0.75	64°	97°

6 Implications of the extended-MFV model for $b \to d\gamma$ transitions

In this section we study the implications of the extended–MFV model on the observables related to the exclusive

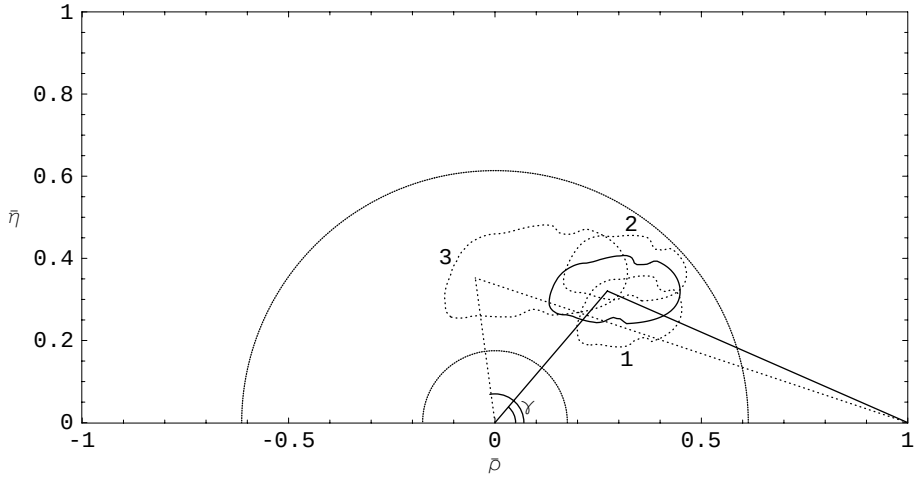

Fig. 8. Allowed 95% C.L. contours in the $(\bar\rho, \bar\eta)$ plane. The solid contour is the SM case. The two semicircles represent the 2 σ region allowed by $|V_{ub}/V_{cb}| = 0.090 \pm 0.025$. The contours numbered 1 to 3 correspond respectively to the points indicated in Fig. 5 a, and their (g_R, g_I) values are given in Table 2. Note that the UT–contour 3 yields $\gamma > \pi/2$

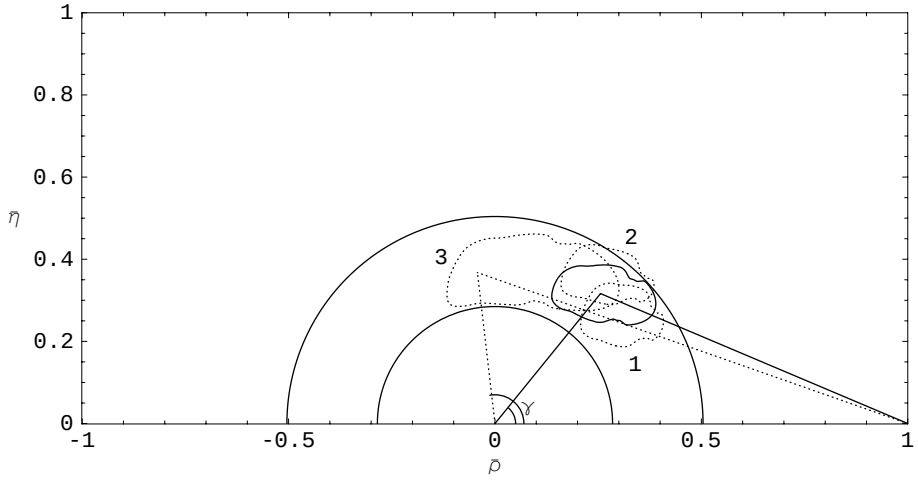

Fig. 9. The same as in Fig. 8. The error on $|V_{ub}/V_{cb}|$ is reduced by a factor of 2. The two semicircles represent the 2 σ region allowed by $|V_{ub}/V_{cb}| = 0.090 \pm 0.0125$. The (g_R, g_I) values corresponding to the three extended–MFV contours are given in Table 3

decays $B \to \rho\gamma$, namely the ratio $R(\rho\gamma/K^*\gamma)$ defined in (40), the isospin breaking ratio

$$\Delta = \frac{\Delta^{+0} + \Delta^{-0}}{2}\,, \tag{61}$$

where

$$\Delta^{\pm 0} = \frac{\mathcal{B}(B^\pm \to \rho^\pm\gamma)}{2\mathcal{B}(B^0 \to \rho^0\gamma)} - 1\,, \tag{62}$$

and the CP asymmetry

$$A_{CP} = \frac{\mathcal{B}(B^- \to \rho - \gamma) - \mathcal{B}(B^+ \to \rho^+\gamma)}{\mathcal{B}(B^- \to \rho - \gamma) + \mathcal{B}(B^+ \to \rho^+\gamma)}\,. \tag{63}$$

We perform the numerical analysis for following set of SUSY input parameters (that satisfy all the constraints previously discussed): $\mu = 120$ GeV, $M_2 = 350$ GeV, $\tan\beta = 4$, $M_{\tilde t_2} = 280$ GeV, $\theta_{\tilde t} = -0.29$ and $M_{H^\pm} = 290$ GeV. This allows us to exploit in detail the dependence of the various observables on the phase of the mass insertion and to give an illustrative example of the modifications in the profile of these quantities.

In Fig. 10 we plot the ratio $R(\rho\gamma/K^*\gamma)$ as a function of $\arg\delta_{\tilde t_2 \tilde u_L}$ in the Extended-MFV model, and compare the resulting estimates with the SM estimates, shown by the two dashed lines representing the 1σ SM predictions. The solid curves are the SUSY results obtained for ρ and η set to their central values and for $|\delta_{\tilde u_L \tilde t_2}| = \delta^{\rm lim}$, 0.55 and 0.25.

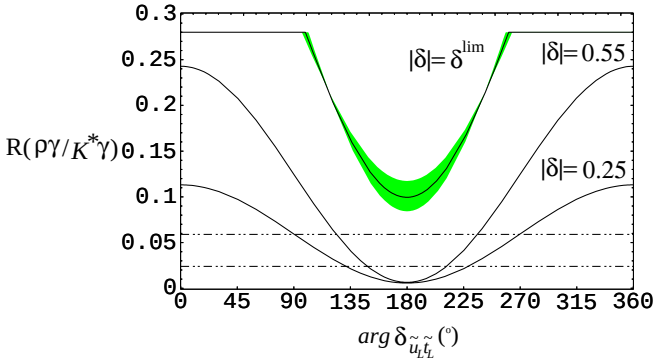

Fig. 10. The ratio $R(\rho\gamma/K^*\gamma) = \mathcal{B}(B \to \rho\gamma)/\mathcal{B}(B \to K^*\gamma)$ as a function of $\arg\delta_{\tilde t_2 \tilde u_L}$ (in degrees) in the Extended-MFV model, satisfying the present experimental upper bound $R(\rho\gamma/K^*\gamma) < 0.28$ (at 90% C.L.). The solid lines are obtained for $\bar\rho$ and $\bar\eta$ set to their central values and for $|\delta_{\tilde u_L \tilde t_2}| = \delta^{\rm lim}$, 0.55 and 0.25. The shaded region in the top curve represents the 1 σ uncertainty due to the fit of the unitarity triangle. The dashed lines indicate the 1 σ SM prediction

Here, $\delta^{\rm lim}$ is the absolute value of the mass insertion that saturates the experimental upper bound $R < 0.28$; it is required to be smaller than 1 and it depends on the phase of the mass insertion. For the point that we consider, it varies between 0.6 (for $\arg \delta_{\tilde{t}_2\tilde{u}_L} = 0, \pi$) and 1. The shaded region shown for the $|\delta_{\tilde{u}_L\tilde{t}_2}| = \delta^{\rm lim}$ represents the 1 σ uncertainty in the CKM-parameters $(\bar{\rho}, \bar{\eta})$ resulting from the fit of the unitarity triangle. In the maximal insertion case, the experimental upper bound $R(\rho\gamma/K^*\gamma) < 0.28$ is saturated for $\arg \delta_{\tilde{t}_2\tilde{u}_L} \in [0, \pi/2] \cup [3\pi/2, 2\pi]$. Note that if we require the absolute value of the insertion to be maximal, the ratio $R(\rho\gamma/K^*\gamma)$ is always larger than in the SM. We point out that, in the extended–MFV model, this ratio does not show a strong dependence on the ρ and η values as long as these CKM parameters remain reasonably close to their allowed region. On the other hand, the impact of reducing $|\delta_{\tilde{t}_2\tilde{u}_L}|$ is quite significant.

Taking into account the discussion at the end of Sect. 3 and that $C_7^s(m_b)$ is negative for all the points that allow for a sizable mass insertion contribution, the $\arg \delta_{\tilde{t}_2\tilde{u}_L}$ region in which the experimental bound on $R(\rho\gamma/K^*\gamma)$ is saturated turns out to be strongly dependent on the sign of $\overline{C}_7^{MI}$. Moreover, a large $\overline{C}_7^{MI}$ is usually associated with a large stop mixing angle whose sign determines, therefore, the overall sign of the mass insertion contribution. In our case, $\overline{C}_7^{MI} < 0$ and the region $\mathrm{Re}\, \delta_{\tilde{t}_2\tilde{u}_L} > 0$ is consequently favoured. The qualitative behaviour of this plot can be understood rewriting (46) as

$$R(\rho\gamma/K^*\gamma) = R^{SM}|1 + Ae^{i \arg \delta}|^2 = R^{SM}[1 + A^2 + 2A\cos(\arg \delta)] \quad (64)$$

where $A \equiv |\delta_{\tilde{t}_2\tilde{u}_L}|\eta^{16/23}\overline{C}_7^{MI}/C_7^s(m_b)$ is positive for the point we consider.

The explicit expressions for the isospin breaking ratio and the CP asymmetry in the SM are [81]

$$\Delta_{LO} = 2\epsilon_A \left[F_1 + \frac{1}{2}\epsilon_A(F_1^2 + F_2^2)\right] , \quad (65)$$

$$A_{CP} = -\frac{2F_2(A_I^u - \epsilon_A A_I^{(1)t})}{C_7^{SM}(m_b)(1 + \Delta_{LO})} \quad (66)$$

where $\epsilon_A = -0.3$, $A_I^u = 0.046$, $A_I^{(1)t} = -0.016$ and

$$F_1 = \mathrm{Re}\, \frac{V_{ub}V_{ud}^*}{V_{tb}V_{td}^*} \equiv -\left|\frac{V_{ub}V_{ud}^*}{V_{tb}V_{td}^*}\right| \cos\alpha , \quad (67)$$

$$F_2 = \mathrm{Im}\, \frac{V_{ub}V_{ud}^*}{V_{tb}V_{td}^*} \equiv -\left|\frac{V_{ub}V_{ud}^*}{V_{tb}V_{td}^*}\right| \sin\alpha . \quad (68)$$

Note that ϵ_A is proportional to $1/C_7^{SM}(m_b)$. Equations (65) and (66) can be easily extended to the supersymmetric case by means of the following prescriptions:

$$V_{td}^* \to V_{td}^* \exp\{i \arg C_7^d(m_b)\} \quad [\text{i.e.: } \alpha \to \alpha - \arg C_7^d(m_b)] , \quad (69)$$

$$C_7^{SM}(m_b) \to |C_7^d(m_b)| . \quad (70)$$

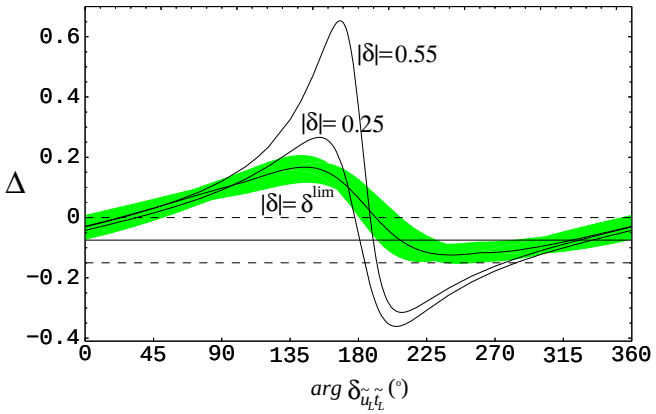

Fig. 11. The isospin breaking ratio Δ as a function of $\arg \delta_{\tilde{t}_2\tilde{u}_L}$ (in degrees). See the caption in Fig. 10 for further explanations

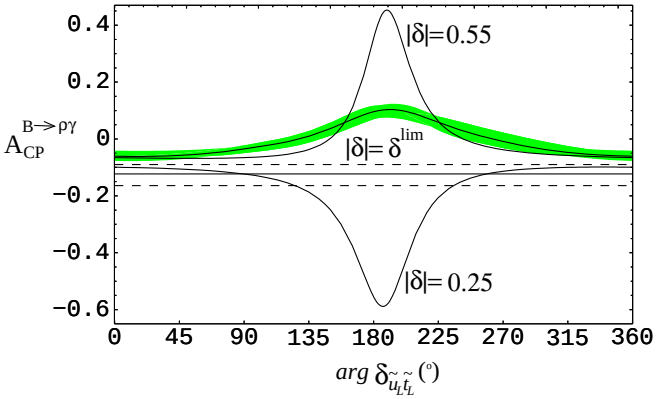

Fig. 12. The CP asymmetry in $B^\pm \to \rho^\pm\gamma$ as a function of $\arg(\delta_{\tilde{t}_2\tilde{u}_L})$ (in degrees). See the caption in Fig. 10 for further explanations

In Figs. 11 and 12 we present the results of the analysis for the isospin breaking ratio and of the CP asymmetry in $B^\pm \to \rho^\pm\gamma$, respectively, for the three representative cases: $|\delta_{\tilde{u}_L\tilde{t}_2}| = \delta^{\rm lim}$, 0.55 and 0.25 in the Extended-MFV model and compare them with their corresponding SM-estimates. Since, in all likelihood, the measurement of the ratio $R(\rho\gamma/K^*\gamma)$ will precede the measurement of either Δ or the CP-asymmetry in $B \to \rho\gamma$ decays, the experimental value of this ratio and the CP-asymmetry $a_{\psi K_S}$ can be used to put bounds on $|\delta|$ and $\arg \delta_{\tilde{u}_L\tilde{t}_2}$. The measurements of Δ and the CP-asymmetry in $B^\pm \to \rho^\pm\gamma$ will then provide consistency check of this model. Concerning the cases $|\delta_{\tilde{u}_L\tilde{t}_2}| = 0.55$ and 0.25, we must underline that large deviations occur in the phase range in which an unobservably small $R(\rho\gamma/K^*\gamma)$ is predicted. On the other hand, it is interesting to note that, for the case of maximal insertion and for a phase compatible with the measurements of $a_{\psi K_S}$ (see Fig. 7), sizable deviations from the SM can occur for the CP asymmetry but not for the isospin breaking ratio.

7 Summary and conclusions

The measured CP asymmetry $a_{\psi K_S}$ in B decays is in good agreement with the SM prediction. It is therefore very likely that this CP asymmetry is dominated by SM effects. Yet, the last word on this consistency will be spoken only after more precise measurements of $a_{\psi K_S}$ and other CP–violating quantities are at hand. It is possible that a consistent description of CP asymmetries in B–decays may eventually require an additional CP-violating phase. With that in mind, we have investigated an extension of the so–called Minimal Flavour Violating version of the MSSM, and its possible implications on some aspects of B physics. The non–CKM structure in this Extended-MFV model reflects the two non–diagonal mass insertions from the squark sector which influence the FCNC transitions $b \to d$ and $b \to s$ (see (11)). In the analysis presented here, we have assumed that the main effect of the mass insertions in the B-meson sector is contained in the $b \to d$ transition. This is plausible based on the CKM pattern of the $b \to d$ and $b \to s$ transitions in the SM. The former, being suppressed in the SM, is more vulnerable to beyond-the-SM effects. This assumption is also supported by the observation that the SM contribution in $b \to s\gamma$ decays almost saturates the present experimental measurements. We remark that the assumption of neglecting the mass insertion $(\delta_{\tilde{c}_L \tilde{t}_2})$ can be tested in the CP-asymmetry in the $b \to s$ sector, such as $\mathcal{A}_{\rm CP}(B \to X_s\gamma)$, $\mathcal{A}_{\rm CP}(B \to K^*\gamma)$, the B_s^0 - $\overline{B_s^0}$ mass difference ΔM_{B_s}, and more importantly through the induced CP-asymmetry in the decay $B_s^0(\overline{B_s^0}) \to J/\psi\phi$, which could become measurable in LHC experiments [37] due to the complex phase of $(\delta_{\tilde{c}_L \tilde{t}_2})$. The parameters of the model discussed here are thus the common mass of the heavy squarks and gluino $(M_{\tilde{q}})$, the mass of the lightest stop $(M_{\tilde{t}_2})$, the stop mixing angle $(\theta_{\tilde{t}})$, the ratio of the two Higgs vevs $(\tan\beta_S)$, the two parameters of the chargino mass matrix (μ and M_2), the charged Higgs mass $(M_{H^\pm})$ and the complex insertion $(\delta_{\tilde{u}_L \tilde{t}_2})$.

We have shown that, as far as the analysis of the unitarity triangle is concerned, it is possible to encode all these SUSY effects in the present model in terms of two real parameters (f and g_R) and an additional phase emerging from the imaginary part of g (g_I). We find that despite the inflation of supersymmetric parameters from one (f in the MFV models) to three (in the Extended-MFV models), the underlying parameter space can be effectively constrained and the model remains predictive. We have worked out the allowed region in the plane $(f, |g| = |g_R + i g_I|)$ by means of a high statistic scatter plot scanning the underlying supersymmetric parameter space, where the allowed parametric values are given in (48). The experimental constraints on the parameters emerging from the branching ratios of the decays $B \to X_s\gamma$ and $B \to \rho\gamma$ (implemented via the ratio $R(\rho\gamma/K^*\gamma)$), as well as from the recent improved determination of the magnetic moment of the muon $(g-2)_\mu$ were taken into account, whereby the last constraint is used only in determining the sign of the μ-term.

We have done a comparative study of the SM, the MFV-models and the Extended-MFV model by performing a χ^2-analysis of the unitarity triangle in which we have included the current world average of the CP asymmetry $a_{\psi K_S}$ ((3)) and the current lower bound $\Delta M_{B_s} > 14.9\ {\rm ps}^{-1}$ using the amplitude method. Requiring the minimum of the χ^2 to be less than two, we were able to define allowed-regions in the (g_R, g_I) plane (correlated with the value of f), which are significantly more restrictive than the otherwise allowed ranges for $|g|$. We studied the dependence of the CP-asymmetry $a_{\psi K_S}$ on the phase of the mass insertion $(\delta_{\tilde{u}_L \tilde{t}_2})$ and find that, depending on this phase, it is possible to get both SM/MFV-like solutions for $a_{\psi K_S}$, as well as higher values for the CP-asymmetry. We constrain this phase to lie in the range $0^\circ \le \arg\delta_{\tilde{u}_L \tilde{t}_2} \le 100^\circ$, which typically yields the Extended–MFV phase θ_d to lie in the range $-3^\circ \le \theta_d \le 8^\circ$. The assumed measurement of the mass difference ΔM_{B_s}, when inserted in the χ^2 analysis, further restricts the allowed regions in $|g|$. However, as ΔM_{B_s} has not yet been measured, this part of the analysis is mostly illustrative. Finally, we have shown the profile of the resulting CKM–Unitarity triangle for some representative values in the extended–MFV model. They admit solutions for which $a_{\psi K_S} > a_{\psi K_S}^{\rm SM}$ and $\gamma > \gamma^{\rm SM}$, favoured by present data.

To test our model, we have focused on three observables sensitive to the mass insertion $(\delta_{\tilde{u}_L \tilde{t}_2})$ related to the radiative decays $B \to \rho\gamma$. We have worked out the consequences of the present model for the quantities $R(\rho\gamma)/R(K^*\gamma) = 2\mathcal{B}(B^0 \to \rho^0\gamma)/\mathcal{B}(B^0 \to K^{*0}\gamma)$, the isospin violating ratio $\Delta^{\pm 0} = \mathcal{B}(B^\pm \to \rho^\pm\gamma)/2\mathcal{B}(B^0 \to \rho^0\gamma) - 1$, and direct CP-asymmetry in the decay rates for $B \to \rho\gamma$ and its charge conjugate. We conclude that the partial branching ratios in $B \to \rho\gamma$, and hence also the ratio $R(\rho\gamma/K^*\gamma)$ can be substantially enhanced in this model compared to their SM-based values. The CP-asymmetry can likewise be enhanced compared to the SM value, and more importantly, it has an opposite sign for most part of the parameter space. On the other hand, it is quite difficult to obtain a significant isospin breaking ratio without suppressing the branching ratios themselves.

Finally, we remark that our analysis has led us to an interesting observation: the requirement of a positive magnetic moment Wilson coefficient (i.e., $C_7^s > 0$), entering in $b \to s\gamma$ and $b \to s\ell^+\ell^-$ decays, is found to be incompatible with a sizable contribution to the parameter g, which encodes, in the present model, the non–CKM flavour changing contribution. Thus, it is possible to distinguish two different scenarios depending on the sign of C_7^s. In the $C_7^s < 0$ case, as in the SM, only small deviations in the $b \to s$ phenomenology are expected, but sizable contributions to g_R and g_I are admissible, thereby leading to striking effects in the $b \to d$ sector. On the other hand, a positive C_7^s will have strong effects in the $b \to s$ sector but, since $|g|$ will be highly constrained, the model being studied becomes a limiting case of the MFV models. In particular, in this scenario, no appreciable change in the CP-asymmetry $a_{\psi K_s}$ compared to the SM/MFV cases is anticipated. Since the experimental value of $a_{\psi K_S}$ [(3)] is in agreement with the SM/MFV–models, configurations in which $a_{\psi K_S}$ receives small corrections have a slight pref-

erence over the others. These aspects will be decisively tested in B-factory experiments.

Acknowledgements. E.L. acknowledges financial support from the Alexander Von Humboldt Foundation. We would like to thank Riccardo Barbieri, Fred Jegerlehner, David London, Antonio Masiero and Ed Thorndike for helpful discussions and communications.

Appendix

A Stop and chargino mass matrices

The 2×2 stop mass matrix is given by

$$M^2_{\tilde{t}} = \begin{pmatrix} M^2_{\tilde{t}_{LL}} & M^2_{\tilde{t}_{LR}} \\ M^2_{\tilde{t}_{LR}} & M^2_{\tilde{t}_{RR}} \end{pmatrix} \tag{71}$$

where

$$M^2_{\tilde{t}_{LL}} = M^2_{\tilde{q}} + \left(\frac{1}{2} - \frac{2}{3}\sin^2\theta_W\right)\cos 2\beta_S\, M^2_Z + M^2_t \ , \tag{72}$$

$$M^2_{\tilde{t}_{RR}} = M^2_{\tilde{q}} + \frac{2}{3}\sin^2\theta_W \cos 2\beta_S\, M^2_Z + M^2_t \ , \tag{73}$$

$$M^2_{\tilde{t}_{LR}} = M_t|A_t - \mu^* \cot(\beta_S)| \ . \tag{74}$$

The eigenvalues are given by

$$2M^2_{\tilde{t}_1,\tilde{t}_2} = (M^2_{\tilde{t}_{LL}} + M^2_{\tilde{t}_{RR}}) \pm\sqrt{(M^2_{\tilde{t}_{LL}} - M^2_{\tilde{t}_{RR}})^2 + 4(M^2_{\tilde{t}_{LR}})^2} \ , \tag{75}$$

with $M^2_{\tilde{t}_2} \le M^2_{\tilde{t}_1}$. We parametrize the mixing matrix $\mathcal{R}^{\tilde{t}}$ so that

$$\begin{pmatrix} \tilde{t}_1 \\ \tilde{t}_2 \end{pmatrix} = \mathcal{R}^{\tilde{t}} \begin{pmatrix} \tilde{t}_L \\ \tilde{t}_R \end{pmatrix} = \begin{pmatrix} \cos\theta_{\tilde{t}} & \sin\theta_{\tilde{t}} \\ -\sin\theta_{\tilde{t}} & \cos\theta_{\tilde{t}} \end{pmatrix} \begin{pmatrix} \tilde{t}_L \\ \tilde{t}_R \end{pmatrix} \ . \tag{76}$$

The chargino mass matrix

$$M^{\tilde{\chi}^+}_{\alpha\beta} = \begin{pmatrix} M_2 & M_W\sqrt{2}\sin\beta_S \\ M_W\sqrt{2}\cos\beta_S & \mu \end{pmatrix} \tag{77}$$

can be diagonalized by the bi-unitary transformation

$$\tilde{U}^*_{j\alpha} M^{\tilde{\chi}^+}_{\alpha\beta} \tilde{V}^*_{k\beta} = M_{\tilde{\chi}^+_j}\delta_{jk} \ , \tag{78}$$

where $\tilde{U}$ and $\tilde{V}$ are unitary matrices such that $M_{\tilde{\chi}^+_j}$ are positive and $M_{\tilde{\chi}^+_1} < M_{\tilde{\chi}^+_2}$.

B Loop functions

The loop functions for box diagrams, entering in ε_K, ΔM_{B_d} and ΔM_{B_s}, are,

$$\begin{aligned} &G(a,b) \\ &= -\frac{ab}{4}\left(\frac{a^2-8a+4}{(a-b)(a-1)^2}\ln a + \frac{b^2-8b+4}{(b-a)(b-1)^2}\ln b \right. \\ &\quad \left. -\frac{3}{(a-1)(b-1)}\right) \ , \\ &Y_1(a,b,c,d) \\ &= \frac{a^2}{(b-a)(c-a)(d-a)}\ln a \\ &\quad + \frac{b^2}{(a-b)(d-b)(d-b)}\ln b \\ &\quad + \frac{c^2}{(a-c)(b-c)(d-c)}\ln c \\ &\quad + \frac{d^2}{(a-d)(b-d)(c-d)}\ln d \ , \\ &Y_2(a,b,c,d) \\ &= \sqrt{4cd}\left[\frac{a}{(b-a)(c-a)(d-a)}\ln a \right. \\ &\quad + \frac{b}{(a-b)(c-b)(d-b)}\ln b \\ &\quad + \frac{c}{(a-c)(b-c)(d-c)}\ln c \\ &\quad \left. + \frac{d}{(a-d)(b-d)(c-d)}\ln d\right] \ , \\ &Y_1^{MI}(a,b,c,d) \\ &= \frac{Y_1(a,a,c,d) + Y_1(b,b,c,d) - 2Y_1(a,b,c,d)}{(a-b)^2} \ . \end{aligned}$$

The loop functions for penguin diagrams, entering in $b \to (s,d)\gamma$ and in the anomalous magnetic moment of the muon, are

$$\begin{aligned} F_1(x) &= \frac{x^3 - 6x^2 + 3x + 2 + 6x\ln x}{12(x-1)^4} \ , \\ F_3(x) &= \frac{x^2 - 4x + 3 + 2\ln x}{2(x-1)^3} \ , \\ f_1(x) &= \frac{-7 + 12x + 3x^2 - 8x^3 + 6x(-2+3x)\ln x}{6(x-1)^4} \ , \\ f_2(x) &= \frac{5 - 12x + 7x^2 - 2x(-2+3x)\ln x}{2(x-1)^3} \ , \\ f^{MI}_{1,2}(x,y) &= \frac{f_{1,2}(x) - f_{1,2}(y)}{(x-y)} \ . \end{aligned} \tag{79}$$

References

1. N. Cabibbo, Phys. Rev. Lett. **10**, 531 (1963), M. Kobayashi, T. Maskawa, Prog. Theor. Phys. **49**, 652 (1973)
2. B. Aubert et al. [BABAR Collaboration], hep-ex/0107013
3. K. Abe et al. [BELLE Collaboration], hep-ex/0107061

4. K. Ackerstaff et al. [OPAL Collaboration], Eur. Phys. J. **C5**, 379 (1998), [hep-ex/9801022]
5. T. Affolder et al. [CDF Collaboration], Phys. Rev. **D61**, 072005 (2000), [hep-ex/9909003]
6. C. A. Blocker [CDF Collaboration], To be published in the proceedings of 3rd Workshop on Physics and Detectors for DAPHNE (DAPHNE 99), Frascati, Italy, 16-19 Nov 1999
7. R. Barate et al. [ALEPH Collaboration], Phys. Lett. **B492**, 259 (2000), [hep-ex/0009058]
8. C. Bozzi [BABAR Collaboration], (2001), hep-ex/0103046
9. K. Abe et al. [BELLE Collaboration], Phys. Rev. Lett. **86**, 3228 (2001), [hep-ex/0011090]
10. LEP-B-OSCILLATION Working Group, (http://lepbosc.web.cern.ch/LEPBOSC/), Results for the Winter 2001 Conferences (XXXVIth Rencontres de Moriond: Electroweak Interactions and Unified Theories, March 10-17, 2001)
11. Particle Data Group, D. E. Groom et al., Eur. Phys. J. **C15**, 1 (2000)
12. S. Mele, Phys. Rev. **D59**, 113011 (1999), [hep-ph/9810333]
13. S. Plaszczynski, M.-H. Schune, (1999), hep-ph/9911280
14. M. Bargiotti et al., Riv. Nuovo Cim. **23N3**, 1 (2000), [hep-ph/0001293]
15. A. Ali, D. London, Eur. Phys. J. **C18**, 665 (2001), [hep-ph/0012155]
16. M. Ciuchini et al., (2000), [hep-ph/0012308]
17. A. J. Buras, (2001), hep-ph/0101336
18. D. Atwood, A. Soni, Phys. Lett. **B508**, 17 (2001), [hep-ph/0103197]
19. A. Hocker, H. Lacker, S. Laplace, F. L. Diberder, (2001), hep-ph/0104062
20. A. L. Kagan, M. Neubert, Phys. Lett. **B492**, 115 (2000), [hep-ph/0007360]
21. J. P. Silva, L. Wolfenstein, Phys. Rev. **D63**, 056001 (2001), [hep-ph/0008004]
22. G. Eyal, Y. Nir, G. Perez, JHEP **08**, 028 (2000), [hep-ph/0008009]
23. M. Ciuchini, G. Degrassi, P. Gambino, G. F. Giudice, Nucl. Phys. **B534**, 3 (1998), [hep-ph/9806308]
24. A. Ali, D. London, Eur. Phys. J. **C9**, 687 (1999), [hep-ph/9903535]
25. A. Ali, D. London, Phys. Rept. **320**, 79 (1999), [hep-ph/9907243]
26. A. J. Buras, P. Gambino, M. Gorbahn, S. Jager, L. Silvestrini, Phys. Lett. **B500**, 161 (2001), [hep-ph/0007085]
27. A. J. Buras, R. Buras, Phys. Lett. **B501**, 223 (2001), [hep-ph/0008273]
28. A. Bartl et al., (2001), hep-ph/0103324
29. A. J. Buras, R. Fleischer, (2001), hep-ph/0104238
30. T. Nihei, Prog. Theor. Phys. **98**, 1157 (1997), [hep-ph/9707336]
31. T. Goto, Y. Okada, Y. Shimizu, (1999), hep-ph/9908499
32. T. Goto, Y. Y. Keum, T. Nihei, Y. Okada, Y. Shimizu, Phys. Lett. **B460**, 333 (1999), [hep-ph/9812369]
33. S. Baek, P. Ko, Phys. Rev. Lett. **83**, 488 (1999), [hep-ph/9812229]
34. A. G. Cohen, D. B. Kaplan, F. Lepeintre, A. E. Nelson, Phys. Rev. Lett. **78**, 2300 (1997), [hep-ph/9610252]
35. J. P. Silva, L. Wolfenstein, Phys. Rev. **D55**, 5331 (1997), [hep-ph/9610208]
36. L. Wolfenstein, Phys. Rev. Lett. **51**, 1945 (1983)
37. P. Ball et al., (2000), hep-ph/0003238
38. D. A. Demir, A. Masiero, O. Vives, Phys. Rev. Lett. **82**, 2447 (1999), [hep-ph/9812337]
39. S. Baek, J. H. Jang, P. Ko, J. H. Park, Phys. Rev. **D62**, 117701 (2000), [hep-ph/9907572]
40. L. J. Hall, V. A. Kostelecky, S. Raby, Nucl. Phys. **B267**, 415 (1986)
41. D. Cassel [CLEO Collaboration], talk presented at the XX International Symposium on Lepton and Photon Interactions at High Energies, Rome, Italy, Jul. 23-28, 2001. (To be published in the proceedings)
42. R. Barate et al. [ALEPH Collaboration], Phys. Lett. **B429**, 169 (1998)
43. K. Abe et al. [BELLE Collaboration], Phys. Lett. B **511** (2001) 151 [hep-ex/0103042]
44. H. N. Brown et al. [Muon g-2 Collaboration], Phys. Rev. Lett. **86**, 2227 (2001), [hep-ex/0102017]
45. A. Abashian et al. [BELLE Collaboration], BELLE-CONF-0003 (2000)
46. H. Wahl [NA48 Collaboration], A new measurement of direct CP–violation by NA48 (DESY Seminar, 26/06/2001)
47. A. Glazov [KTeV Collaboration], New measurement of the direct CP–violating parameter Re ϵ'/ϵ by the KTeV Collaboration (DESY Seminar, 19/06/2001)
48. W.-S. Hou, K.-C. Yang, Phys. Rev. Lett. **84**, 4806 (2000), [hep-ph/9911528]
49. M. Beneke, G. Buchalla, M. Neubert, C. T. Sachrajda, (2001), hep-ph/0104110
50. D. Cronin-Hennessy et al. [CLEO Collaboration], Phys. Rev. Lett. **85**, 515 (2000)
51. L. Cavolo [BABAR Collaboration], Talk presented at the XXXVIth Rencontres de Moriond, Electroweak Interactions and Unified Theories, Les Arcs, France, March 2001
52. T. Ijima [BELLE Collaboration], Talk presented at the International Conference on B Physics and CP Violation (BCP4), se–Shima, Japan, 19-23 February 2001
53. A. J. Buras, A. Romanino, L. Silvestrini, Nucl. Phys. **B520**, 3 (1998), [hep-ph/9712398]
54. J. A. Casas, S. Dimopoulos, Phys. Lett. **B387**, 107 (1996), [hep-ph/9606237]
55. E. Lunghi, A. Masiero, I. Scimemi, L. Silvestrini, Nucl. Phys. **B568**, 120 (2000), [hep-ph/9906286]
56. K. Chetyrkin, M. Misiak, M. Münz, Phys. Lett. **B400**, 206 (1997), Erratum-ibid. B **425** (1997) 414, [hep-ph/9612313]
57. M. Ciuchini, G. Degrassi, P. Gambino, G. F. Giudice, Nucl. Phys. **B527**, 21 (1998), [hep-ph/9710335]
58. G. Degrassi, P. Gambino, G. F. Giudice, JHEP **12**, 009 (2000), [hep-ph/0009337]
59. M. Carena, D. Garcia, U. Nierste, C. E. M. Wagner, Phys. Lett. **B499**, 141 (2001), [hep-ph/0010003]
60. A. J. Buras, P. H. Chankowski, J. Rosiek, L. Slawianowska, hep-ph/0107048
61. A. Czarnecki, W. J. Marciano, Nucl. Phys. Proc. Suppl. **76**, 245 (1999), [hep-ph/9810512]; (2001), hep-ph/0102122
62. W. J. Marciano, B. L. Roberts, (2001), hep-ph/0105056
63. M. Davier, A. Hocker, Phys. Lett. **B435**, 427 (1998), [hep-ph/9805470]
64. S. Eidelman, F. Jegerlehner, Z. Phys. **C67**, 585 (1995), [hep-ph/9502298]; S. Eidelman, F. Jegerlehner, Nucl. Phys. Proc. Suppl. 51C, 131 (1996), [hep-ph/9606484]

65. F. Jegerlehner, (2001), hep-ph/0104304
66. S. Narison, Phys. Lett. **B513** 53, (2001), [hep-ph/0103199]
67. T. Moroi, Phys. Rev. **D53**, 6565 (1996), [hep-ph/9512396]
68. T. Ibrahim, P. Nath, Phys. Rev. **D61**, 095008 (2000), [hep-ph/9907555]; T. Ibrahim, P. Nath, Phys. Rev. **D61**, 015004 (2000), [hep-ph/9908443]
69. L. L. Everett, G. L. Kane, S. Rigolin, L.-T. Wang, Phys. Rev. Lett. **86**, 3484 (2001), [hep-ph/0102145]
70. J. L. Feng, K. T. Matchev, Phys. Rev. Lett. **86**, 3480 (2001), [hep-ph/0102146]
71. E. A. Baltz, P. Gondolo, (2001), hep-ph/0102147
72. U. Chattopadhyay, P. Nath, (2001), hep-ph/0102157
73. S. Komine, T. Moroi, M. Yamaguchi, Phys. Lett. **B506**, 93 (2001), [hep-ph/0102204]
74. J. Ellis, D. V. Nanopoulos, K. A. Olive, (2001), hep-ph/0102331
75. R. Arnowitt, B. Dutta, B. Hu, Y. Santoso, Phys. Lett. **B505**, 177 (2001), [hep-ph/0102344]
76. S. P. Martin, J. D. Wells, (2001), hep-ph/0103067
77. D. F. Carvalho, J. Ellis, M. E. Gomez, S. Lola, (2001), hep-ph/0103256
78. H. Baer, C. Balazs, J. Ferrandis, X. Tata, (2001), hep-ph/0103280
79. CLEO, T. E. Coan et al., Phys. Rev. Lett. **84**, 5283 (2000), [hep-ex/9912057]
80. A. Ali, V. M. Braun, H. Simma, Z. Phys. **C63**, 437 (1994), [hep-ph/9401277]
81. A. Ali, L. T. Handoko, D. London, Phys. Rev. **D63**, 014014 (2000), [hep-ph/0006175]
82. A. Khodjamirian, G. Stoll, D. Wyler, Phys. Lett. **B358**, 129 (1995), [hep-ph/9506242]
83. A. Ali, V. M. Braun, Phys. Lett. **B359**, 223 (1995), [hep-ph/9506248]
84. A. Ali, A. Y. Parkhomenko, (2001), hep-ph/0105302
85. S. W. Bosch, G. Buchalla, (2001), hep-ph/0106081
86. P. Cho, M. Misiak, D. Wyler, Phys. Rev. **D54**, 3329 (1996), [hep-ph/9601360]
87. A. Ali, P. Ball, L. T. Handoko, G. Hiller, Phys. Rev. **D61**, 074024 (2000), [hep-ph/9910221]
88. F. Krüger, E. Lunghi, Phys. Rev. **D63**, 014013 (2001), [hep-ph/0008210]
89. A. J. Buras, M. E. Lautenbacher, G. Ostermaier, Phys. Rev. **D50**, 3433 (1994), [hep-ph/9403384]
90. A. J. Buras, M. Jamin, P. H. Weisz, Nucl. Phys. **B347**, 491 (1990)
91. S. Herrlich, U. Nierste, Nucl. Phys. **B419**, 292 (1994), [hep-ph/9310311]
92. S. Herrlich, U. Nierste, Phys. Rev. **D52**, 6505 (1995), [hep-ph/9507262]
93. T. Draper, Nucl. Phys. Proc. Suppl. **73**, 43 (1999), [hep-lat/9810065]
94. S. R. Sharpe, (1998), hep-lat/9811006
95. C. Bernard, Nucl. Phys. Proc. Suppl. **94**, 159 (2001), [hep-lat/0011064]
96. C. Bernard et al., Phys. Rev. Lett. **81**, 4812 (1998), [hep-ph/9806412]
97. H. G. Moser, A. Roussarie, Nucl. Instrum. Meth. **A384**, 491 (1997)
98. P. Checchia, E. Piotto, F. Simonetto, (1999), hep-ph/9907300
99. G. Boix, D. Abbaneo, JHEP **08**, 004 (1999), [hep-ex/9909033]; M. Ciuchini et al., (2000), hep-ph/0012308
100. Heavy Flavour Steering Group, http://lephfs.web.cern.ch/LEPHFS
101. B. H. Behrens et al. [CLEO Collaboration], Phys. Rev. D **61** (2000) 052001 [hep-ex/9905056]